JBC RESEARCH ARTICLE

MRCKβ links Dasm1 to actin rearrangements to promote dendrite development

Received for publication, December 12, 2020, and in revised form, April 23, 2021 Published, Papers in Press, April 30, 2021,
https://doi.org/10.1016/j.jbc.2021.100730

Xiao-Xiao Wang[1,2,‡], **Si Zhang**[1,‡], **Ping-Ping Dong**[2,3,‡], **Yao-Hua Li**[1], **Li Zhang**[1], **Song-Hai Shi**[4,5], **Zhi-Qiang Yu**[6,7,*], **and She Chen**[1,*]

From the [1]NHC Key Laboratory of Glycoconjugate Research, Department of Biochemistry and Molecular Biology, School of Basic Medical Sciences, [2]Department of Gastroenterology and Hepatology, Shanghai Institute of Liver Diseases, Zhongshan Hospital, Fudan University, Shanghai, China; [3]Department of Surgery, Faculty of Medicine, Centre for Cancer Research, The University of Hong Kong, Hong Kong, China; [4]IDG/McGovern Institute for Brain Research, Tsinghua-Peking Center for Life Sciences, Beijing Frontier Research Center of Biological Structure, Beijing Advanced Innovation Center for Structural Biology, School of Life Sciences, Tsinghua University, Beijing, China; [5]Developmental Biology Program, Sloan Kettering Institute, Memorial Sloan Kettering Cancer Center, New York, New York, USA; [6]NHC Key Laboratory of Myopia, Chinese Academy of Medical Sciences, Shanghai, China; and [7]Eye Department, Eye & ENT Hospital, Fudan University, Shanghai, China

Edited by Roger Colbran

Proper dendrite morphogenesis and synapse formation are essential for neuronal development and function. Dasm1, a member of the immunoglobulin superfamily, is known to promote dendrite outgrowth and excitatory synapse maturation *in vitro*. However, the *in vivo* function of Dasm1 in neuronal development and the underlying mechanisms are not well understood. To learn more, *Dasm1* knockout mice were constructed and employed to confirm that Dasm1 regulates dendrite arborization and spine formation *in vivo*. We performed a yeast two-hybrid screen using Dasm1, revealing MRCKβ as a putative partner; additional lines of evidence confirmed this interaction and identified cytoplasmic proline-rich region (823–947 aa) of Dasm1 and MRCKβ self-activated kinase domain (CC1, 410–744 aa) as necessary and sufficient for binding. Using co-immunoprecipitation assay, autophosphorylation assay, and BS3 cross-linking assay, we show that Dasm1 binding triggers a change in MRCKβ's conformation and subsequent dimerization, resulting in autophosphorylation and activation. Activated MRCKβ in turn phosphorylates a class 2 regulatory myosin light chain, which leads to enhanced actin rearrangement, causing the dendrite outgrowth and spine formation observed before. Removal of Dasm1 in mice leads to behavioral abnormalities. Together, these results reveal a crucial molecular pathway mediating cell surface and intracellular signaling communication to regulate actin dynamics and neuronal development in the mammalian brain.

Dendrites are long and highly branched extensions from the neuronal cell body. They can receive, integrate, and process synaptic inputs terminating either on the dendritic shaft or spine (1, 2). Precise transduction of neuronal signal relies on the proper development of dendritic structures that consists mainly of five fundamental steps: neurites extension; dendrites polarization; dendrites outgrowth and branching; spine formation; dendrites pruning and synaptic remolding (3). Proper dendrite morphology is regulated by various extrinsic signals, including secreted cues (protein ligands, like Netrins and Slits *et al.*), contacted-mediated cues (adhesion proteins, like Dscam *et al.*), and neuronal activity (calcium signaling, like CAMKs *et al.*), as well as by intracellular pathways, such as cytoskeletal remodeling molecules, secretory pathways, transcription factors, and RNA molecules (4). During dendritic development, neuronal cell surface receptors receive extracellular cues, followed by interpreting interpret these signals to intracellular pathways and eventually generate distinct dendrite patterns (4, 5). However, dendritic-specific cell surface receptors responsible for signal transmission remain largely elusive.

The immunoglobulin superfamily (IgSF), one of the most abundant cell surface receptors in the nervous system, modulates intrinsic pathways through the interaction between its intracellular domains and its partners (6). Previously, we have demonstrated that Dasm1, an evolutionarily conserved member of the IgSF, promotes dendrite outgrowth (7) and excitatory synapse maturation (8) in cultured hippocampal neurons. However, their underlying molecular mechanisms are largely unknown. Dasm1 has a large extracellular domain (N-terminal signal sequence, five immunoglobulin [Ig]-like domains, and two fibronectin type III domains); a transmembrane domain; and a long C-terminal cytoplasmic tail containing proline-rich region (PRR) domain (7). The structure of the extracellular domain of Dasm1 is similar to that of the cell-surface receptors Robo/Dutt1 and DCC/Frazzled/UNC-40 (7). Dendrite growth is impaired by treating neurons with a truncated form of Dasm1 (7), which lacks the intracellular portion and is unable to interact with its intracellular partners, indicating that Dasm1 specifically mediates an unexplored intracellular signaling pathway to regulate dendritic growth. Dasm1 may serve as a cell surface receptor

‡ These authors contributed equally to this work.
* For correspondence: She Chen, shechen@fudan.edu.cn; Zhi-Qiang Yu, zhiqiang.yu@fdeent.org.

to transmit signals into cells for dendrite development. Further study of the Dasm1 intracellular pathway could provide direct insight into the Dasm1 function.

As mentioned above, the intracellular structure of Dasm1 contains a PRR. The PRR domain can be commonly in multiple actin regulatory proteins to bind to the WWP repeating motif (WW) domain and the Src homology 3 domain (9, 10). These interactions can translate extracellular cues into intracellular cytoskeleton dynamics. The actin cytoskeleton contributes to the development of neurite growth cones, to the dynamic plasticity of dendritic spines, and to the formation of periodic lattice within the dendrite shaft, thus providing structural support for proper dendrite development (11). In particular, during the protrusion of the neurite growth cone, the adhesive substrate links to the actin cytoskeleton, and F-actin is polymerized to push the membrane forward, which leads to the extension of the growth cone (11, 12). F-actin mainly forms parallel filaments in the neck of the dendritic spine and lattice or twisted filaments in the head of the dendritic spine (13). In addition, the existence of ~190 nm periodic lattice actin cytoskeleton has been observed in the dendritic shaft and spine head, and, hence, this configuration may participate in shaping and maintaining dendritic morphology (14–16). The role of the actin cytoskeleton in dendrite development has been extensively studied (13). However, the key elements responsible for its regulation are still not fully understood.

Here, we found that adolescent *Dasm1*$^{-/-}$ mice harbor decreased dendritic complexity, less spine formation, and behavioral abnormalities. Dasm1 PRR domain bound to myotonic dystrophy-related Cdc42-binding kinases beta (MRCKβ), a key regulator of the actin–myosin cytoskeleton (17) and functions as a switch to trigger the conformation change of MRCKβ, subsequently increasing its activity. Activated MRCKβ promoted actin rearrangement *via* the phosphorylation of class 2 regulatory myosin light chains (MLC2), eventually leading to dendrite growth and spine formation.

Results

Impaired dendrite arborization and spine formation in Dasm1 knockout mice

We previously found that suppression of *Dasm1* with RNA interference impaired dendrite outgrowth in cultured hippocampal neurons (7). To further explore the specificity of RNAi-mediated *Dasm1* knockdown, we co-transfected *Dasm1* shRNA with full-length wild-type *Dasm1* (*Dasm1*-WT) or full-length shRNA-resistant *Dasm1* (*Dasm1*-Resistant) into cultured hippocampal neurons. We found that *Dasm1* shRNA-impaired dendritic outgrowth was rescued by the *Dasm1*-Resistant, but not by the *Dasm1*-WT plasmid (Fig. S1, *A*–*C*). Furthermore, overexpression of Dasm1 promoted dendrite outgrowth, indicated by a significant increase in dendrite length (Fig. S2, *A*–*C*) and branches (Fig. S2, *A*, *B* and *D*) on day 6 *in vitro* (6 DIV), 10 DIV, and 25 DIV. Sholl analysis showed that the dendrite arbor was more complex in neurons overexpressing Dasm1 at 10 DIV (Fig. S2*E*). Overexpression of Dasm1 dramatically increased spine density (Fig. S2, *F* and *G*) and spine maturation indicated by an increased proportion of mushroom spines and a reduced proportion of thin spines in cultured neurons (Fig. S2*J*), without altering spine length (Fig. S2*H*) or width (Fig. S2*I*). Together, these results suggest that Dasm1 specifically regulates dendrite arborization and spine morphogenesis *in vitro*.

To further determine the *in vivo* role of Dasm1 in dendritic morphogenesis, we generated *Dasm1* knockout mice by homologous recombination in embryonic stem cells (Fig. S3). Gross anatomy in brains and the numbers of neurons and neuroglia cells in the hippocampus were not noticeably altered (Fig. S4) in *Dasm1*$^{-/-}$ mice. Neuronal dendrite morphology was then quantified by Golgi staining (Fig. 1, *A* and *B*), and *Dasm1*$^{-/-}$ mice showed decreased proximal dendrites (Fig. 1, *A* and *B*) and simplified dendritic arbors at postnatal day 30 (P30; Fig. 1*E*). Decreased total dendrite length (Fig. 1*C*) and branches (Fig. 1*D*) were found in early postnatal (P) life (P10, P15, and P30) but not in the late postnatal life (P60) in *Dasm1*$^{-/-}$ mice. Consistently, dendrite complexity, as well as dendrite length and branches, was markedly reduced in primary hippocampal neurons cultured from *Dasm1*$^{-/-}$ mice (Fig. S5, *A*–*E*).

Furthermore, we measured spine morphology in hippocampal pyramidal neurons from *Dasm1*$^{-/-}$ mice at P30 (Fig. 1*F*) and found that Dasm1 knockout dramatically decreased spine density (Fig. 1*G*) without altering spine length (Fig. 1*H*) or width (Fig. 1*I*). *Dasm1* knockout dramatically decreased the proportion of mushroom spines and increased the proportion of thin spines at P30 (Fig. 1*J*), indicating that loss of Dasm1 inhibits spine maturation. Nevertheless, the decreased spine density and the impaired spine maturation were restored in *Dasm1*$^{-/-}$ mice at P60 (Fig. S5, *F*–*J*). Together, these results indicated that Dasm1 ensures a proper dendritic development, including the dendritic arbor and spine formation, both *in vitro* and *in vivo*.

Interaction of Dasm1 PRR with the MRCKβ CC1 domain

The structure of Dasm1 renders it capable of serving as a potential neuronal cell-surface receptor and of transducing outside signal into intracellular pathway controlling dendrite development (18). To dissect the Dasm1-mediated intracellular signaling pathway, we conducted yeast two-hybrid screen to identify Dasm1's intracellular signaling partner. After ruling out various Dasm1 C-terminal fragments because of their autotranscriptional activity, the Dasm1 intracellular PRR fragment, which comprises amino acid residues 823 to 974, was chosen as a bait (Fig. S6). A ~0.9 kb MRCKβ fragment was then identified as the interacting partner of the Dasm1 PRR domain. Dasm1 and MRCKβ were co-localized in both HeLa cells and neurons (Fig. 2*A*). The endogenous association between Dasm1 and MRCKβ was then confirmed by co-immunoprecipitation assay in the brain lysates of mice (Fig. 2*B*). Furthermore, Dasm1 interacted with MRCKβ and MRCKγ, but not with MRCKα in HEK293T cells (Fig. 2*C*).

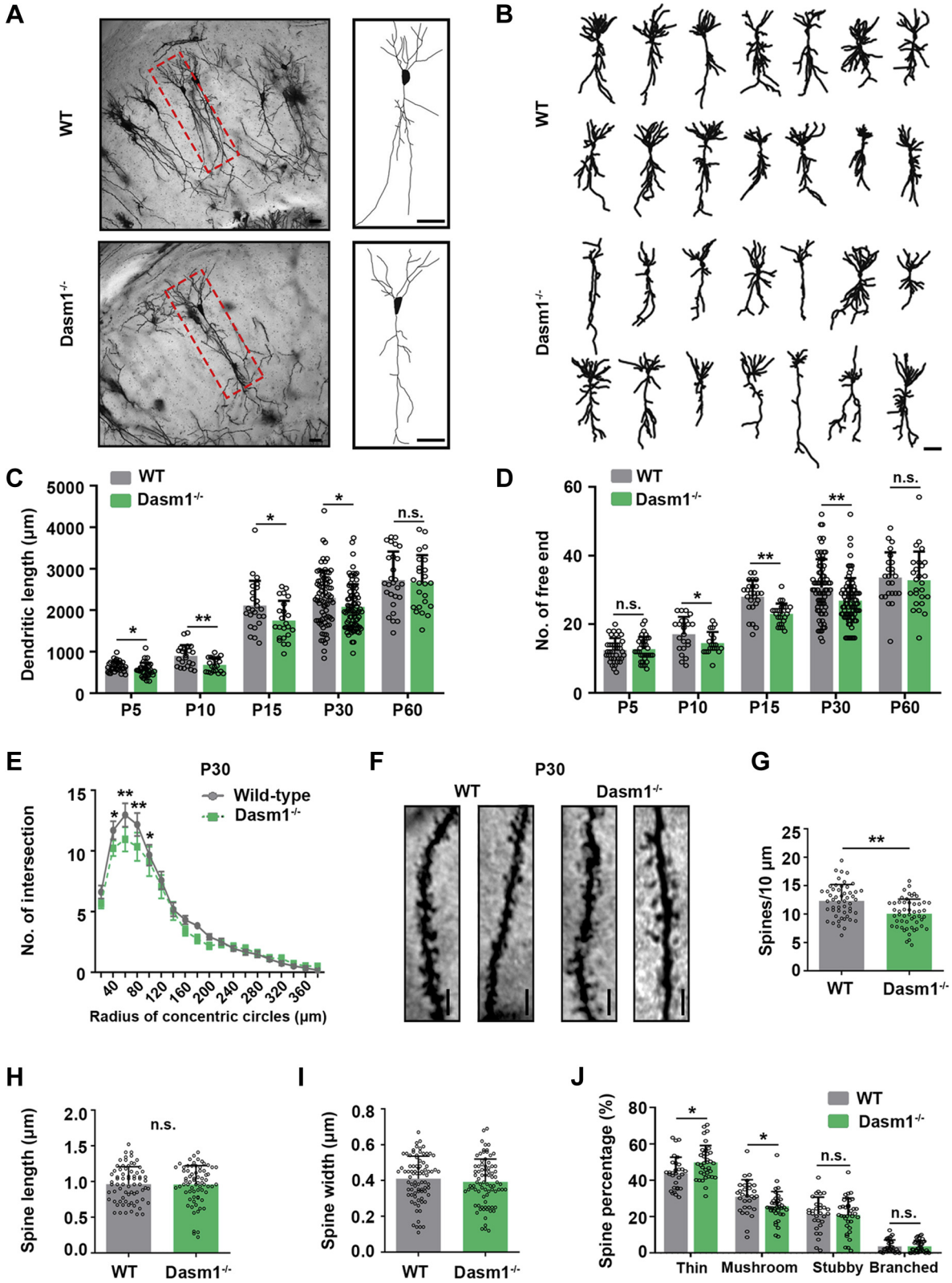

Figure 1. Dasm1 knockout inhibits dendrite arborization and spine formation in mice. *A*, representative images of Golgi-stained hippocampal pyramidal neurons in *Dasm1*$^{-/-}$ mice and WT littermates. Scale bar, 50 μm. *B*, morphometric reconstruction of hippocampal pyramidal neurons in *Dasm1*$^{-/-}$ mice and WT littermates. Scale bar, 100 μm. *C*, *Dasm1*$^{-/-}$ mice displayed decreased total dendritic length of hippocampal pyramidal neurons fixed at postnatal (P) 5, P10, P15, and P30, but not P60, compared with WT littermates. Results were expressed as mean ± SD; n = 30 to 35; *$p < 0.05$, **$p < 0.01$, n.s., not significant; Unpaired two-tailed *t* test. *D*, *Dasm1*$^{-/-}$ mice displayed less branches of hippocampal pyramidal neurons fixed at P10, P15, and P30, but not P60, compared with WT littermates. Results were expressed as mean ± SD; n = 20 to 83; *$p < 0.05$, **$p < 0.01$, n.s., not significant; Unpaired two-tailed *t* test. *E*, Sholl analysis showed that *Dasm1*$^{-/-}$ mice displayed a reduced dendritic complexity of hippocampal pyramidal neurons at P30. Concentric circles with a 20 μm spacing were drawn around cell body, and the intersection number of all dendritic branches with the circles was counted. Results were expressed as

Owing to a low association between MRCKγ and Dasm1 (Fig. 2*C*) as well as the strict expression of MRCKγ in cardiac and skeletal muscle (19), we mainly focused on the interaction between MRCKβ and Dasm1 in this study. We further identified that Dasm1 PRR is required for Dasm1's association with MRCKβ, proved by the fact that deletion of this region impaired the association (Fig. 2*D*). And, the MRCKβ CC1 domain (amino-acid residues 410–744), a kinase self-activation region (20), was sufficient for the Dasm1/MRCKβ interaction (Fig. 2*E*).

We found that *in vitro*–translated MRCKβ was pulled down by purified GST-Dasm1 PRR fusion protein (Fig. 2*F*, left panel). *In vitro*–translated Dasm1 was pulled down by purified GST-MRCKβ CC1 fusion protein and by GST-MRCKβ (1–939) fusion protein (Fig. 2*F*, right panel). These results suggest a direct interaction between Dasm1 and MRCKβ. A computational 3D complex structural model by FR-t5-M, FALCON, and ZDock based on the X-ray crystal structure from the Protein Data Bank was further generated (Fig. 2*G*). Docking simulation data from the model demonstrated that amino acids GLU-54, TRP-58, PHE-409, LEU-415, LYS-416, and GLN-431 of MRCKβ form a "hairpin" structure (Fig. 2*H*, left panel), and that amino acids ARG-772, VAL-859, ALA-860, SER-862, GLN-863, LYS-865, ALA-911, PRO-932, and LEU-934 of Dasm1 form a "hairpin" structure (Fig. 2*H*, right panel). The 3D structure of Dasm1/MRCKβ complex illustrated that these two "hairpin" structures were responsible for the interaction of Dasm1 and MRCKβ (Fig. 2*G*). To bolster the interaction evidence from the 3-D predictions, we generated Myc-tagged Dasm1-PRR (Myc-PRR-mut) and HA-tagged MRCKβ CC1 (HA-CC1-mut) plasmids carrying multiple point mutation based on the 3-D predictions. Myc-PRR-mut stands for Myc-Dasm1-PRR $^{(R772A,\ V859A,\ A860G,\ S862A,\ Q863A,\ K865A,\ A911G,\ P932A,\ L934A)}$. HA-CC1-mut stands for HA-MRCKβ CC1 $^{(E54A,\ W58A,\ F409A,\ L415A,\ K416A,\ Q431A)}$. As shown in Figure 2*H*, HA-CC1-mut lost the binding ability with Dasm1-PRR (Lane 3) and significantly weakened interaction between mutant Dasm1 PRR and WT MRCKβ CC1 was observed (Lane 4), suggesting essential amino acids for the interaction between Dasm1 and MRCKβ are among these sites.

Dasm1 facilitates MRCKβ activation via *opening MRCKβ's closed conformation*

It is well known that MRCKβ kinase phosphorylates MLC2 at Thr18/Ser19 (17, 21). To test whether Dasm1/MRCKβ interaction affects MRCKβ kinase activity, we performed the *in vitro* kinase activity assay (Fig. 3*A*) (21). We found that MRCKβ activity, indicated by the phosphorylation level of GST-MLC2 on Ser19 and Thr18 residues, was increased when Dasm1 was co-purified with MRCKβ (Fig. 3*B*). Consistently, the level of phosphorylated MLC2 was significantly increased in Dasm1-overexpressing HeLa cells (Fig. 3, *C* and *E*, left panel), whereas it was markedly reduced in *Dasm1*$^{-/-}$ mice (Fig. 3, *D* and *E*, right panel). Together, these data indicate that Dasm1 interacts with MRCKβ, thereby promoting MRCKβ's kinase activity.

The basis of MRCKβ's autoinhibitory mechanism is the intramolecular interaction of the kinase region (CAT) with the CC2/3 domain, which forms a closed conformation. Opening this closed conformation leads to MRCKβ's intermolecular dimerization, autophosphorylation, and subsequent kinase activation (20). In support of our hypothesis that Dasm1-mediated MRCKβ activation may rely on MRCKβ's conformation change, we found that Dasm1 weakened the intramolecular interaction between MRCKβ's CAT and CC domain (containing CC1, CC2, and CC3) in Dasm1-overexpressing HEK293T cells (Fig. 3*F*, left panel; Fig. 3*F*, right panel). This effect relies on the interaction between Dasm1 and the MRCKβ CC1 domain, as deletion of the MRCKβ CC1 region abolished the influence of Dasm1 on the interaction between MRCKβ's CAT and CC2-3 domain (containing CC2 and CC3, but not CC1) in Dasm1-overexpressing HEK293T cells (Fig. 3*F*, middle panel; Fig. 3*F*, right panel). Furthermore, we found that Dasm1 significantly increased MRCKβ's autophosphorylation (Fig. 3*G*) and dimerization (Fig. 3*H*) in Dasm1-overexpressing HeLa cells. Together, these data indicated that Dasm1 disrupts the MRCKβ intramolecular interaction *via* its interaction with the MRCKβ CC1 domain, thereby allowing MRCKβ's autophosphorylation, dimerization, and subsequent activation (Fig. 3*I*).

MRCKβ kinase activity is required for Dasm1-regulated dendrite arborization and spine formation

We found that overexpression of full-length MRCKβ and MRCKβ 1 to 430 (kinase domain) increased dendrite overgrowth and complexity (Fig. 4, *A*–*C*) and spine density and maturation (Fig. 4, *D*–*H*), whereas overexpression of MRCKβ K105M (kinase-inactive mutant) decreased dendrite development, suggesting that MRCKβ-promoted dendrite morphogenesis is kinase activity-dependent. Furthermore, the overexpression of full-length MRCKβ and MRCKβ 1 to 430 (kinase domain) rescued the defects in dendrite arborization (Fig. 5, *A*–*C*), and spine formation (Fig. 5, *D*–*H*) induced by *Dasm1* shRNA, whereas the kinase-inactive mutant MRCKβ K105M, at a similar level, failed to rescue this defect. These results demonstrate that MRCKβ's activity is required for the role of Dasm1 in dendrite morphogenesis and spine formation.

mean ± SD; n = 20 to 83; *$p < 0.05$, **$p < 0.01$; two-way ANOVA (Interaction: F (18, 2983) = 70.53, $p < 0.0001$; Row Factor: F (18, 2983) = 8005, $p < 0.0001$; Column Factor: F (1, 2983) = 511.6, $p < 0.0001$). *F*, representative images of hippocampal pyramidal neurons harboring spines in *Dasm1*$^{-/-}$ mice and wild-type littermates fixed at P30. Scale bar, 5 μm. *G*–*I*, quantification of spine morphology of hippocampal pyramidal neurons in *Dasm1*$^{-/-}$ mice and WT littermates. *Dasm1*$^{-/-}$ mice showed decreased spine density (*G*), and unchanged spine length (*H*), and spine width (*I*). Results were expressed as mean ± SD; n = 52 to 81; **$p < 0.01$, n.s., not significant; Unpaired two-tailed *t* test. *J*, *Dasm1*$^{-/-}$ mice showed increased thin spines and decreased mushroom spines. Results were expressed as mean ± SD; n = 30 to 36; *$p < 0.05$, n.s., not significant; two-way ANOVA (Interaction: F (3, 256) = 5.483, $p = 0.0011$; Row Factor: F (3, 256) = 325.7, $p < 0.0001$; Column factor: F (1, 256) = 6.377e-012, $p > 0.9999$). MRCKβ, myotonic dystrophy-related Cdc42-binding kinases beta.

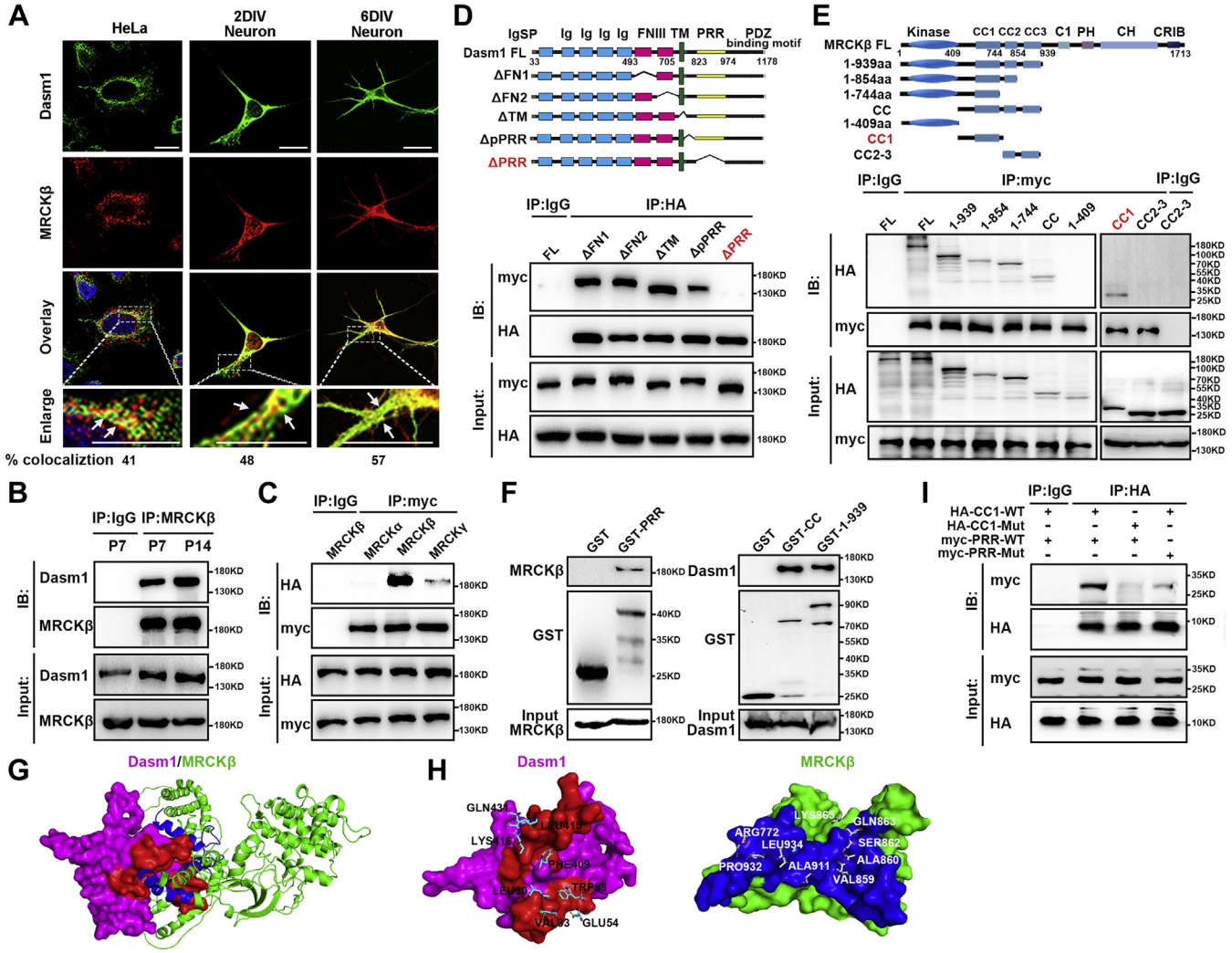

Figure 2. Identification of MRCKβ as a Dasm1 interactor. *A*, confocal immunofluorescence showed co-localization of Dasm1 and MRCKβ in HeLa cells and dissociated hippocampal neurons cultured for 2 or 6 days *in vitro* (2 DIV or 6 DIV). *Upper panel* scale bar, 20 μm; *Middle* scale bar, 10 μm; *Lower panel* scale bar, 40 μm. The "% colocalization" shows the percentage of Dasm1 overlapping with MRCKβ to the total Dasm1. *B*, co-immunoprecipitation of endogenous Dasm1 with MRCKβ in mouse brain lysates. Mouse brain lysates were collected at postnatal (P) 7 and P 14 days and subjected to co-immunoprecipitation assay using indicated antibodies. *C*, co-immunoprecipitation of Dasm1 with abundant MRCKβ and little MRCKγ, but not MRCKα in 293T cells. Myc-tagged Dasm1 was co-expressed with HA-tagged MRCKα, MRCKβ, or MRCKγ in 293T cells, and cell extracts were subjected to co-immunoprecipitation assay using indicated antibodies. Results were from three independent experiments. *D*, Dasm1 bound to MRCKβ *via* its intracellular PRR. *Upper panel*, schematic representation of Dasm1 and various deletion mutants used for mapping Dasm1-binding site. *Lower panel*, HA-tagged MRCKβ was co-expressed with various Myc-tagged Dasm1 deletion mutants in 293T cells as indicated, and cell extracts were subjected to co-immunoprecipitation assay using the indicated antibodies. Text annotation in *red color* indicates the binding site required within Dasm1. *E*, MRCKβ binds to Dasm1 *via* its self-activating kinase domain (CC1, 410–744 amino-acid residues). *Upper panel*, schematic representation of MRCKβ and various truncated mutants used for mapping MRCKβ-binding site. *Lower panel*, Myc-tagged Dasm1 was co-expressed with various HA-tagged MRCKβ truncated mutants in 293T cells as indicated, and cell extracts were subjected to co-immunoprecipitation assay using the indicated antibodies. Text annotation in *red color* indicates the binding site required within MRCKβ. *F*, the direct interaction between Dasm1-PRR and MRCKβ-CC1 was validated by GST pull-down assay. *Left panel*, *in vitro*–translated MRCKβ was pulled down by purified GST-Dasm1-PRR fusion protein. *Right panel*, *in vitro*–translated Dasm1 was pulled down by purified GST-MRCKβ-CC1 or GST-MRCKβ-1 to 939 fusion protein. *G*, the three-dimensional structure of Dasm1/MRCKβ complex in stereo. The structure of MRCKβ 410 to 744 amino-acid residues was depicted in surface (*green*), in which the amino acid residues selected as candidate interfaces were colored with *blue*. The structure of the Dasm1 PRR domain was depicted in surface (*magenta*), in which the amino acid residues selected as candidate interfaces were colored with *red*. *H*, overview of the Dasm1/MRCKβ interface in stereo. *Left panel*, residues of MRCKβ (*red*) which polar contacted to Dasm1 (*magenta*) were depicted in atom-colored stick (*light blue*). *Right panel*, residues of Dasm1 (*blue*) which polar contacted to MRCKβ (*green*) were depicted in atom-colored stick (*white*). *I*, essential amino acids for the interaction between Dasm1 and MRCKβ. We generated Myc-tagged Dasm1-PRR (Myc-PRR-mut) and HA-tagged MRCKβ CC1 (HA-CC1-mut) plasmids carrying multiple point mutation based on the 3-D predictions. Myc-PRR-mut stands for Myc-Dasm1-PRR $^{(R772A,\ V859A,\ A860G,\ S862A,\ Q863A,\ K865A,\ A911G,\ P932A,\ L934A)}$. HA-CC1-mut stands for HA-MRCKβ CC1 $^{(E54A,\ W58A,\ F409A,\ L415A,\ K416A,\ Q431A)}$. Then, co-immunoprecipitation assay was employed to test the interaction. C1, protein kinase C conserved region 1 domain; CC, coil-coiled domain; CH, citron homology domain; CRIB, Cdc42/Rac interactive binding domain; Ig, immunoglobulin domain; FL, full-length; FNIII, Fibronectin III domain; MRCKβ, myotonic dystrophy-related Cdc42-binding kinases beta; PH, Pleckstrin homology-like domain; pPRR, preproline-rich region; PRR, proline-rich region; SP, signal peptide; TM, transmembrane domain.

Dasm1-MRCKβ axis promotes actin rearrangement

Active MRCKβ could regulate actin rearrangement *via* phosphorylation of MLC2 (20). Actin filaments, together with stable microtubule arrays and neurofilaments, form the cytoskeleton in dendrites. After showing that Dasm1-promoted dendrite development depends on MRCKβ activity, we

proceeded to determine whether Dasm1 promotes dendrite development through MRCKβ/MLC2-mediated actin rearrangement. We found that full-length MRCKβ and MRCKβ 1 to 430, but not MRCKβ K105M, could rearrange actin filaments and increase actin-constituted stress fibers in HeLa cells (Fig. 6, *A* and *B*). Similar results were obtained in full-length overexpressing Dasm1 HeLa cells (Fig. 6*C*, lane 2; Fig. 6*D*, lane 2). Furthermore, Dasm1 1 to 974, which contains the intracellular MRCKβ-binding PRR domain, could promote actin rearrangement, whereas Dasm1 ΔPRR (deletion of PRR

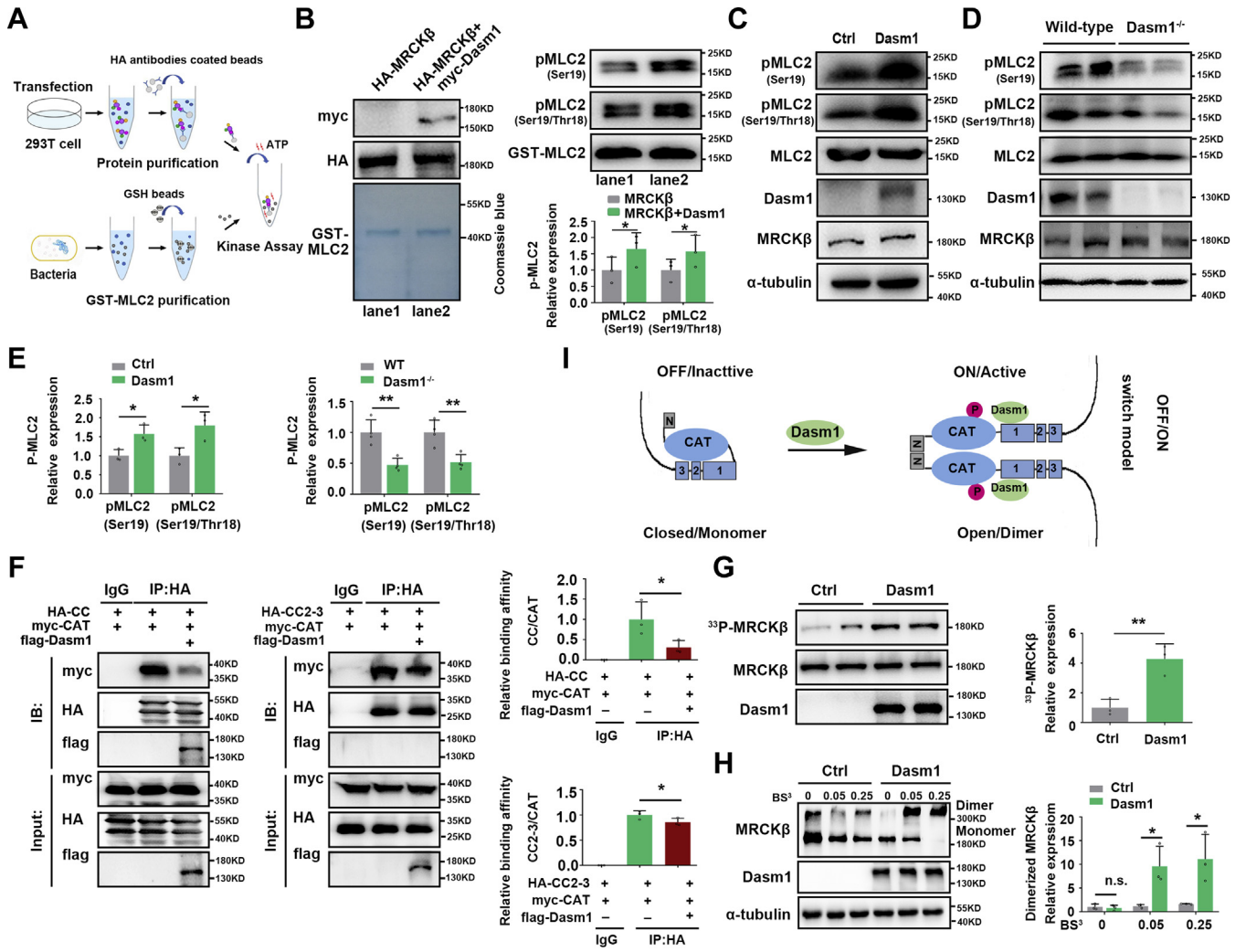

Figure 3. Dasm1 promotes MRCKβ kinase activity. *A*, schematic representation of *in vitro* MRCKβ kinase Assay. HA-tagged MRCKβ or Myc-tagged Dasm1 was expressed in 293T cells and purified with anti-HA tagged or anti-Myc antibody-conjugated protein G coated agarose beads. The GST-MLC2 fusion protein was expressed in BL21 bacterial cells and purified using Glutathione-Sepharose 4B beads. Purified HA-MRCKβ protein alone or a combination of HA-MRCKβ and Myc-Dasm1 protein was added to the kinase reaction system, followed by MRCKβ kinase activity assay using GST-MLC2 as substrate. *B*, *in vitro* MRCKβ kinase Assay showed that HA-MRCKβ incubated with Myc-Dasm1 (lane 2, *left panel*; lane 2, *right panel*) presented higher kinase activity than HA-MRCKβ incubated alone (lane 1, *left panel*; lane 1, *right panel*). *Left panel*, protein used in the kinase activity assay was verified by Western blotting and Coomassie Blue Staining. *Right panel*, MRCKβ kinase activity was determined as the phosphorylation level of its substrate MLC2. Results were expressed as mean ± SD; n = 3; $*p < 0.05$, n.s., not significant; Unpaired two-tailed test. *C*, Dasm1 overexpressing promoted MLC2 phosphorylation on Ser19 and Thr18 residues in HeLa cells. *D*, knockout of Dasm1 inhibited MLC2 phosphorylation on Ser19 and Thr18 residues in brain lysate from mice *in vivo*. *E*, quantification of the immunoblotting results corresponding to *C* (*left panel*) and *D* (*right panel*). Results were expressed as mean ± SD; n = 3 to 4; $*p < 0.05$; $**p < 0.01$; Unpaired two-tailed *t* test. *F*, Dasm1 significantly inhibited intramolecular interaction between MRCKβ kinase domain (CAT) and CC autoinhibitory domain, this effect required the interaction between Dasm1 and MRCKβ CC1. *Left panel*, Dasm1 overexpressing inhibited the interaction between MRCKβ CAT and CC domain in HEK293T cells. *Middle panel*, CC1 domain is required for Dasm1-mediated inhibitory effect on intramolecular interaction between MRCKβ CAT and CC domain. *Right panel*, quantification of the immunoblotting results. Results were expressed as mean ± SD; n = 3; ns, not significant, $*p < 0.05$; one-way ANOVA *C*: (F (2, 6) = 11.00, $p = 0.0098$); *D*: (F (2, 6) = 202.7, $p < 0.0001$). *G*, Dasm1 significantly enhanced MRCKβ autophosphorylation in Dasm1-overexpressing HeLa cells. Autophosphorylation assays were carried out as described in method. *Right panel*, quantification of MRCKβ autophosphorylation level. Results were expressed as mean ± SD; n = 3; $**p < 0.01$; Unpaired two-tailed *t* test. *H*, Dasm1 significantly enhanced MRCKβ dimerization. Extracts from HeLa cells were exposed to increasing concentrations of BS^3 as indicated, and cross-linked products were detected by Western blot with anti-MRCKβ antibody. *Right panel*, quantification of the dimer MRCKβ. Dasm1 significantly enhanced MRCKβ dimerization. Results were expressed as mean ± SD; n = 3; $*p < 0.05$, $**p < 0.01$, n.s., not significant; two-way ANOVA (Interaction: F (2, 12) = 5.567, $p = 0.0195$; Row Factor: F (2, 12) = 6.713, $p = 0.0111$; Column Factor: F (1, 12) = 20.51, $p = 0.0007$). *I*, the proposed "OFF-ON" switch model depicts how Dasm1 regulates MRCKβ catalytic activity. The intramolecular interaction between the Dasm1 CC autoinhibitory domain CC2-CC3 and the kinase domain keeps the kinase in a closed, inactive, and monomeric structure. The interaction between Dasm1 and MRCKβ CC1 domain opens MRCKβ closed loop and allows its N terminus–mediated dimerization, autophosphorylation, and subsequent kinase activation. MLC2, class 2 regulatory myosin light chains; MRCKβ, myotonic dystrophy-related Cdc42-binding kinases beta.

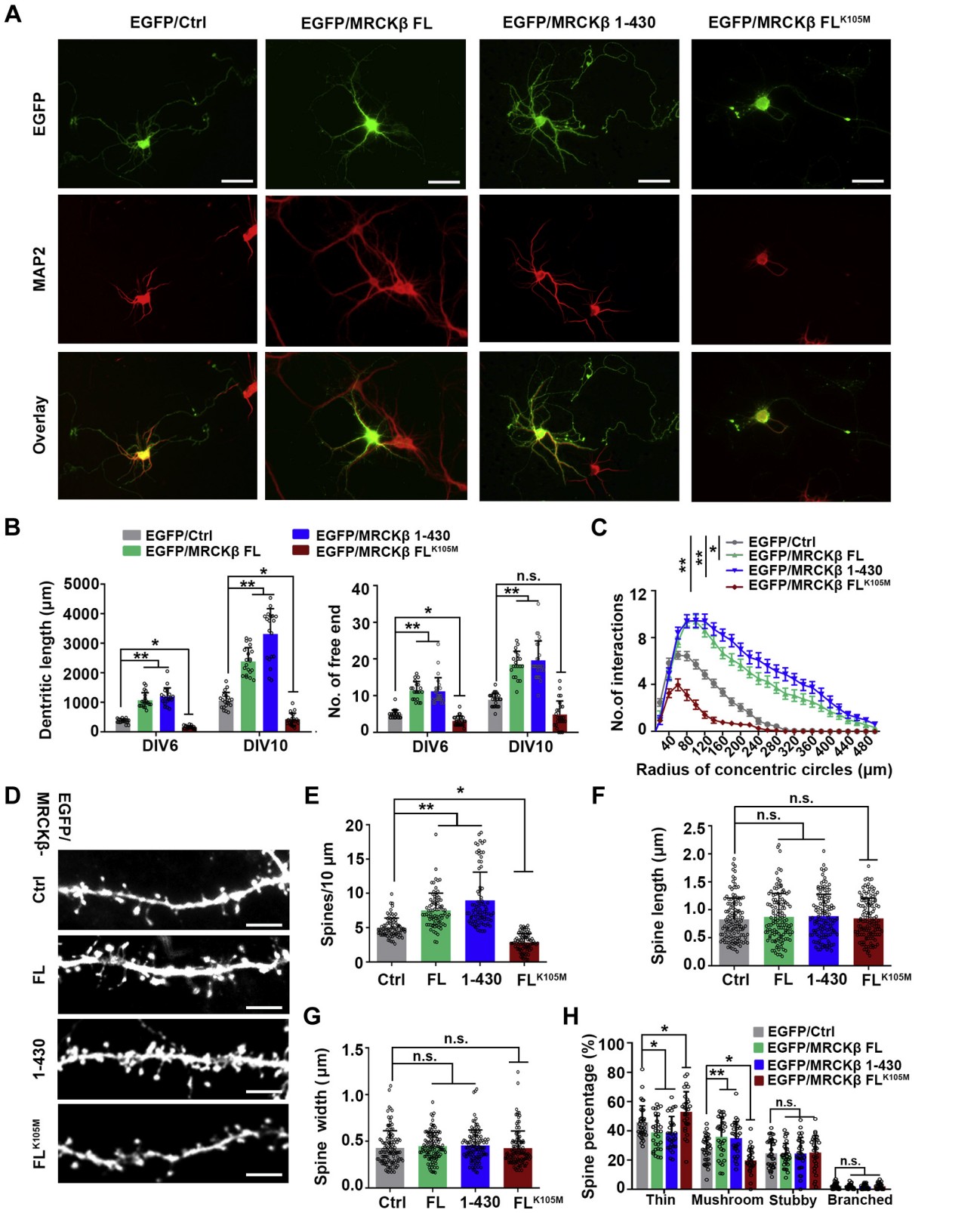

Figure 4. MRCKβ kinase activity is required for dendrite and spine morphogenesis. *A*, representative images of dendrite morphology in dissociated hippocampal neurons. Neurons were transfected with control EGFP (EGFP/Ctrl), EGFP/MRCKβ full-length (FL), EGFP/MRCKβ kinase domain (1–430), or EGFP/MRCKβ kinase-inactive K105M mutant plasmids. Neurons were cultured for 10 days *in vitro* and labeled with antibody against MAP2. Scale bar, 100 μm. *B*, quantification of total dendrite length and branches in neurons transfected with indicated plasmids. Overexpression of MRCKβ FL and MRCKβ 1 to 430 substantially increased dendrite length (*left panel*) and dendrite branches (*right panel*) at 6 DIV, 10 DIV. Overexpression of MRCKβ kinase-inactive K105M mutant significantly decreased dendrite length (*left panel*) and dendrite branches (*right panel*) at 6 DIV. Results were expressed as mean ± SD; n = 20 to 26; *$p < 0.05$, **$p < 0.01$, n.s., not significant; two-way ANOVA; *Left panel*: (Interaction: F (3, 152) = 42.09, $p < 0.0001$; Row Factor: F (1, 152) = 311.3, $p < 0.0001$; Column factor: F (3, 152) = 210.6, $p < 0.0001$). *Right panel*: (Interaction: F (3, 184) = 11.16, $p < 0.0001$; Row Factor: F (1, 184) = 129.7, $p < 0.0001$; Column

region) or Dasm1 1 to 718 (extracellular region) failed to do so (Fig. 6*C*, lane 3–5; Fig. 6*D*, lane 3–5). These results suggest that the binding between Dasm1 and MRCKβ is critical for Dasm1's regulation of actin filaments.

Considering that the actin cytoskeleton-mediated growth cone movement drives dendritic growth (11, 12), we then studied the effect of Dasm1 on actin cytoskeleton in the growth cone. Using N-structured illumination microscopy (N-SIM) super-resolution microscopy, we found that Dasm1 deficiency led to a collapse of the growth cone at 2 DIV (Fig. 7, *A* and *C*) and to a disturbance of the periodic actin lattice, which is a periodic actin ring structure and has been reported to be involved in dendrite morphogenesis (13) at 7 DIV (Fig. 7, *B* and *D*), suggesting that Dasm1 deficiency can disrupt the actin cytoskeleton. Furthermore, both growth cone collapse and actin lattice disturbance induced by Dasm1 deficiency could be restored by overexpression of MRCKβ (Fig. 7, *A–D*), implying that Dasm1-regulated dendritic actin cytoskeleton is mediated *via* MRCKβ.

Learning/memory defects and anxiety/depression-like phenotype in adolescent Dasm1 knockout mice

Proper brain functions, such as learning/memory and mood, require precise dendrite and spine structure integrity (22). To assess the impact of simplified dendritic trees and impaired spine formation on brain functions, we performed a series of behavioral tests on adolescent *Dasm1*$^{-/-}$ mice. Adolescent *Dasm1*$^{-/-}$ mice showed a normal motor function, which was verified by the Rotarod test (Fig. 8*A*). Using the Y-maze test for accessing the working memory ability, we found that spontaneous alternation behavior in adolescent *Dasm1*$^{-/-}$ mice significantly decreased at 48 h, suggesting a long-term working memory impairment (Fig. 8*B*). Spatial learning and memory abilities were assessed using the Morris water maze. In the training phase, adolescent *Dasm1*$^{-/-}$ mice showed a significant impairment in spatial learning, indicated by longer latencies in finding the platform (Fig. 8*C*). In the testing phase, adolescent *Dasm1*$^{-/-}$ mice showed no spatial preference, whereas *WT* mice showed a prominent preference for the target quadrant compared with other quadrants (Fig. 8*D*).

We further evaluated the role of Dasm1 in anxiety-related and depression-related mood using the open-field test, the elevated plus maze test, the tail suspension test, and the forced swimming test. In the open-field test, the adolescent *Dasm1*$^{-/-}$ mice exhibited a significant anxiety-like phenotype, as revealed by the reduction in total distance and number of center zone entries (Fig. 8*E*). In the elevated plus maze test, frequency and time spent in the open arms were significantly decreased in the adolescent *Dasm1*$^{-/-}$ mice (Fig. 8*F*). In addition, we found that the adolescent *Dasm1*$^{-/-}$ mice had longer inactive time in the tail suspension test (Fig. 8*G*) and the forced swim test (Fig. 8*H*), indicating that the adolescent *Dasm1*$^{-/-}$ mice exhibited depression-like behavior. In contrast, we did not find learning and memory defects or anxiety/depression-like phenotype in the adult *Dasm1*$^{-/-}$ mice (Fig. S7), which agrees with our finding that *Dasm1*$^{-/-}$ mice displayed no alteration in dendrite length, branched dendrites (P60; Fig. 1, *C* and *D*), and spine formation (P60; Fig. S5, *F–J*) in the late postnatal life. Together, these results suggest that Dasm1 is critical for brain functions, including learning and memory, and for emotional processes-related behaviors in adolescent mice, but not in adult mice.

Discussion

Here, we uncovered a novel molecular pathway that mediates dendrite outgrowth and spine formation: (1) Dasm1 directly binds to MRCKβ *via* its PRR domain, which triggers MRCKβ conformation change and turns on MRCKβ activity; (2) the Dasm1-MRCKβ-MLC2 axis promotes actin rearrangement, an event leads to dendrite arborization and spine formation; (3) Dasm1-mediated dendrite arborization and spine formation contribute to an adequate performance of brain functions, as shown by the learning and memory defects and anxiety/depression-like behaviors found in the adolescent *Dasm1*$^{-/-}$ mice.

Many PRR-containing proteins play physiological roles in neuronal function by interacting with actin regulatory proteins and translating extracellular cues into intracellular actin dynamics (9, 10). In this context, we discovered that Dasm1 interacted with the intracellular actin regulator MRCKβ *via* its PRR domain. Interestingly, this interaction could turn on the "OFF/ON" switch for MRCKβ activity and leads to subsequent actin rearrangement. MRCKβ kinase has an inactive (OFF) and an active (ON) state. In the inactive (OFF) state, the kinase is usually kept in a monomeric and closed conformation, held by the stable interaction between the kinase domain and the negative autoregulatory coil-coiled (CC) domain CC2-CC3 (20). In the active (ON) state, the kinase is kept in an open structure that facilitates N terminus–mediated dimerization, autophosphorylation, and subsequent kinase activation. Disrupting the interaction between the kinase region and the CC2/3 domain in the inactive (OFF) state can turn on the

factor: F (3, 184) = 155.5, $p < 0.0001$). *C*, Sholl analysis revealed that MRCKβ kinase activity is required for production of dendrite complexity at 10 DIV. Overexpression of MRCKβ FL and MRCKβ 1 to 430 substantially increased dendrite complexity, whereas overexpression of MRCKβ K105M decreased dendrite complexity. Results were expressed as mean ± SEM; n = 20 to 25; *$p < 0.05$, **$p < 0.01$; two-way ANOVA (Interaction: F (72, 2050) = 12.66, $p < 0.0001$; Row Factor: F (24, 2050) = 145.9, $p < 0.0001$; Column factor: F (3, 2050) = 783.8, $p < 0.0001$). *D*, representative images of dendritic spines in 25 DIV neurons transfected with indicated plasmids. Scale bar, 5 μm. *E*, quantification analysis of spine density in neurons transfected with indicated plasmids. Spine density was increased in neurons transfected with MRCKβ FL and MRCKβ 1 to 430, whereas decreased in neurons transfected with MRCKB K105M. Results were expressed as mean ± SD; n = 80; **$p < 0.01$; Kruskal-Wallis test (F (3, 316) = 87.47, $p < 0.0001$). *F* and *G*, spine length (*F*) and width (*G*) were not altered in neurons transfected with full-length MRCKβ or various MRCKβ mutant plasmids. Results were expressed as mean ± SD; n = 114 to 125; n.s., not significant; Kruskal-Wallis test; (*F*): F (3, 496) = 0.5189, $p = 0.6694$). (*G*): F (3, 452) = 0.8247, $p = 0.4807$. *H*, overexpression of MRCKβ FL and MRCKβ 1 to 430 significantly decreased the portion of thin spines and increased the portion of mushroom spines, whereas overexpression of MRCKB K105M increased the portion of thin spines and decreased the portion of mushroom spines. Results were expressed as mean ± SD; n = 30 to 35; *$p < 0.05$, **$p < 0.01$, n.s., not significant; two-way ANOVA (Interaction: F (9, 480) = 11.56, $p < 0.0001$; Row Factor: F (3, 480) = 418.3, $p < 0.0001$; Column factor: F (3, 480) = 1.325e-029, $p > 0.9999$). DIV, day *in vitro*; MRCKβ, myotonic dystrophy-related Cdc42-binding kinases beta.

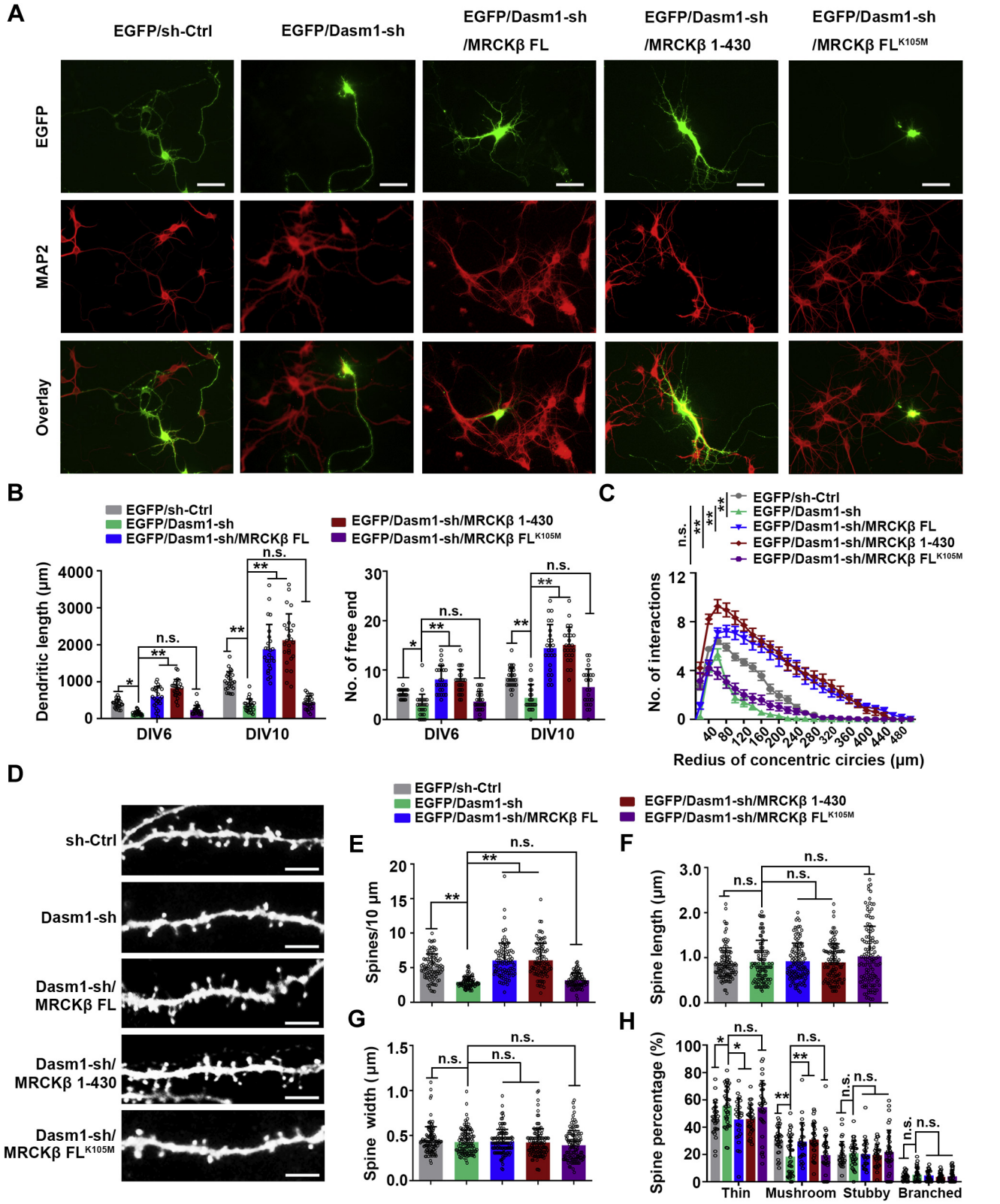

Figure 5. MRCKβ rescues dendrite growth defects caused by Dasm1 suppression. *A*, representative images of dendrite morphology in dissociated hippocampal neurons. Neurons were transfected with control EGFP (EGFP/sh-Ctrl), EGFP/Dasm1-shRNA (sh), and various rescue plasmids including EGFP/MRCKβ full length (FL), EGFP/MRCKβ kinase domain (1–430), and EGFP/MRCKβ kinase-inactive K105M mutant. Neurons were cultured for 10 days *in vitro* and labeled with antibody against MAP2. Scale bar, 100 μm. *B*, quantification of total dendrite length and branches in neurons transfected with the indicated plasmids. MRCKβ FL or MRCKβ 1 to 430, but not MRCKβ K105M, was able to rescue Dasm1 knockdown-induced decrease of total dendrite length (*left panel*) and dendritic branch numbers (*right panel*) in hippocampal neurons. Results were expressed as mean ± SD; n = 25; *$p < 0.05$, **$p < 0.01$, n.s., not significant; two-way ANOVA; *Left panel*: (Interaction: F (4, 240) = 29.82, $p < 0.0001$; Row Factor: F (1, 240) = 260.6, $p < 0.0001$; Column factor: F (4, 240) = 117.4, $p < 0.0001$). *Right panel*: (Interaction: F (4, 240) = 8.838, $p < 0.0001$; Row Factor: F (1, 240) = 136.8, $p < 0.0001$; Column factor: F (4, 240) = 75.53,

"OFF/ON" switch of MRCKβ, as evidenced by the regulation mechanism of Phorbol ester, an exogenous organic compound that binds to the cysteine-rich domain of MRCKβ (23). We further extended these findings and provided the first evidence that Dasm1, as an endogenous protein, can regulate "OFF/ON" switch of MRCKβ activity *via* its interaction with MRCKβ CC1 domain and serve as an endogenously upstream regulator of MRCKβ.

MRCKβ, a key component of cell motility required for cancer cell invasion and metastasis (24), phosphorylates MLC2 at Thr18/Ser19 and subsequently promotes actin-myosin contractility and helps cytoskeleton-tethered transmembrane proteins integrin complexes, to generate tractive forces for cell movement (17, 21, 25). MRCK activity is elevated in invasive and metastatic cancers such as brain cancer, breast cancer, and cervical squamous cell carcinoma (26, 27). Although its role in tumor metastasis has been extensively studied (26–28), the role of MRCKβ in the nervous system remains elusive. Some results have been reported on the roles of its upstream and downstream signals in dendritic morphogenesis (29). For instance, the small GTPase Cdc42, an upstream regulatory molecule of MRCKβ, has been reported to play an essential role in dendrite growth and spine formation (29). Cdc42-mutant vertical system neurons display impaired dendrite and spine morphogenesis, including disrupted dendritic branching, guidance, caliber consistency, and decreased dendritic spine density (29). In addition, myosin IIb, a downstream effector of MRCKβ, is known to be a necessary component of hippocampus-dependent memory formation and synaptic plasticity in the mature nervous system (30). Myosin IIb drives actin filament disassembly, thereby assists in the supply of monomeric actin subunits to F-actin–based structures including spines, actin patches, longitudinal fibers, and rings (13). These structures have been demonstrated to support dendrite shape, to help with protein organization along the plasma membrane, to stabilize the underlying microtubule cytoskeleton, and to influence spine neck elasticity. In line with these findings, we further demonstrated that MRCKβ's activity is required for the role of Dasm1 in dendrite morphogenesis and spine formation.

Appropriate subcellular localizations of MRCKβ, a multi-domain AGC family kinase, is regulated by multiple factors and involves in its kinase activation (19). For instance, Cdc42 binds to MRCKβ CRIB domain, then not only activates MRCKβ but also exposes its ZO-1 binding domain (ZBD, a connecting sequence between the CC3 and C1 domain), consequently ZO-1 anchors the activated enzyme to locate at the leading edge of migrating cells (21). Here, we found that Dasm1 interacted with MRCKβ CC1 domain, unleashed its activity. Meanwhile, we observed their distinct distribution and partial co-localization in neurons. Whether and how Dasm1 may affect MRCKβ localization? It needs further investigation. MRCKβ overexpression only rescued the mushroom spine numbers back to control levels when Dasm1 levels were reduced, despite having a pronounced effect on the overall dendritic arbor. Together, it may suggest that regulation of spine dynamics by MRCKβ requires targeting to specific places within the cell, mediated by Dasm1 interactions. Dasm1 might act as a multifunctional regulator, which not only promotes MRCKβ kinase activation *via* Dasm1/MRCKβ interaction but also directly or indirectly targeting MRCKβ to specific space though conformational changes, such as potentially exposing MRCKβ ZO-1 binding motif (21). In addition, the spine formation and maturation were regulated by multiple factors. Apart from the actin cytoskeleton segments mentioned in our research, spine formation and density can be affected by neuronal activity over both short and long timescales (31). We previously reported that Dasm1 regulated excitatory synapse maturation (8). Overall, it may suggest that MRCKβ rescued the spines density and morphology to control levels *via* a coordinated regulation of cytoskeleton signaling pathway and neuronal activity.

The function of Dasm1 is conserved from *Drosophila* to mammals and regulates a wide variety of central nervous system development (32). In *Drosophila*, the conserved Dasm1 protein Turtle has been implicated in dendrite branching and self-avoidance, photoreceptor axon tiling, and synaptic layer targeting (33–36). The absence of Turtle led to increased degree of its neuronal dendritic crossing points and dendritic branching in class I neurons, with no change in dendritic length in class IV neurons (33, 36). In mammals, we previously reported that Dasm1 can regulate the dendritic outgrowth and excitatory synapse maturation in primary cultured hippocampal neurons (7, 8). Knockdown of Dasm1 by RNA interference or lost most C-terminal amino acids of Dasm1 led to decreased dendritic number (7). Despite the scarcity of studies, the published data on the function of Dasm1 are somewhat contradictory. Mishra *et al.* (37) thought that Dasm1 does not affect brain-derived neurotrophic factor (BDNF)-stimulated dendritic growth and branching in cultured hippocampal neurons. In another study, they found that Dasm1 promoted inhibitory synapse development in CA1 pyramidal neurons *via* homotypic cell aggregation (38). Dasm1$^{-/-}$ mice exhibit increased susceptibility to PTZ-induced seizures, possibly as a

$p < 0.0001$). *C*, Sholl analysis revealed that MRCKβ FL or MRCKβ 1 to 430, but not MRCKβ K105M, was able to rescue Dasm1 knockdown-induced decrease of dendrite complexity at 10 DIV. Results were expressed as mean ± SEM; n = 24 to 25; *$p < 0.05$, **$p < 0.01$; two-way ANOVA(Interaction: F (96, 2975) = 10.49, $p < 0.0001$; Row Factor: F (24, 2975) = 173.5, $p < 0.0001$; Column factor: F (4, 2975) = 449.1, $p < 0.0001$). *D*, representative images of dendritic spines in 25 DIV neurons transfected with indicated plasmids. Scale bar, 5 μm. *E*, quantification analysis of spine density in neurons transfected with indicated plasmids. MRCKβ FL or MRCKβ 1 to 430, but not MRCKβ K105M, was able to rescue Dasm1 knockdown-induced decrease of spine density. Results were expressed as mean ± SD; n = 90; **$p < 0.01$, n.s., not significant; Kruskal-Wallis test (F (4, 445) = 60.23, $p < 0.0001$). *F* and *G*, spine length (*F*) and width (*G*) was not altered in neurons transfected with Dasm1 and various MRCKβ mutants rescue plasmids. Results were expressed as mean ± SD; n =117 to 118; n.s., not significant; Kruskal-Wallis test; (*F*): F (4, 581) = 1.944, $p = 0.1017$; (*G*): F (4, 578) = 2.503, $p = 0.0414$. *H*, MRCKβ FL or MRCKβ 1 to 430, but not MRCKβ K105M, was able to rescue spine immaturation caused by Dasm1 knockdown. Results were expressed as mean ± SD; n = 24 to 35; *$p < 0.05$, **$p < 0.01$, n.s., not significant; two-way ANOVA (Interaction: F (12, 604) = 5.358, $p < 0.0001$; Row Factor: F (3, 604) = 417.7, $p < 0.0001$; Column factor: F (4, 604) = 2.584e-030, $p > 0.9999$). DIV, day *in vitro*; MRCKβ, myotonic dystrophy-related Cdc42-binding kinases beta.

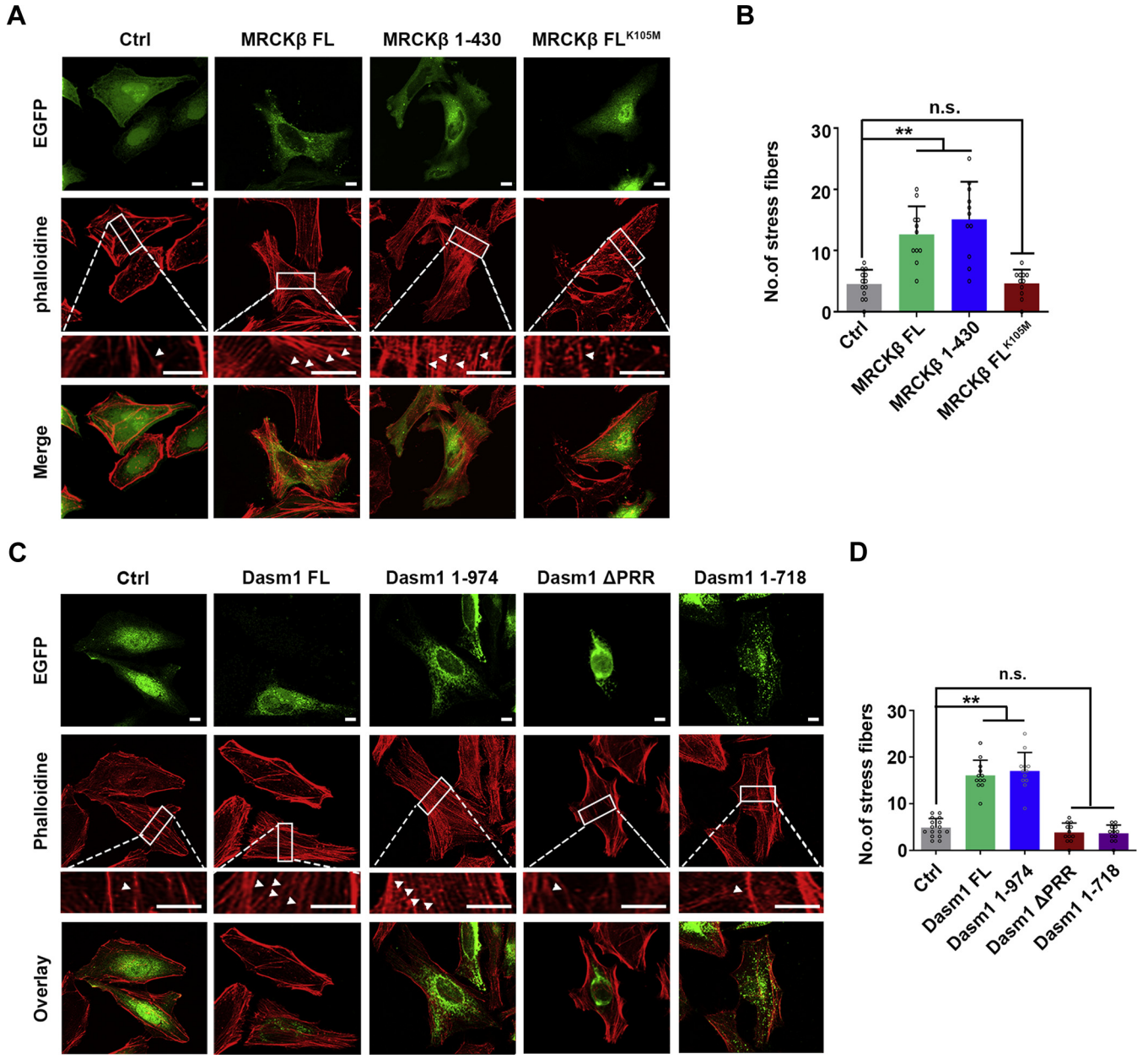

Figure 6. Dasm1-MRCKβ axis promotes stress fiber formation. *A*, MRCKβ promoted stress fiber formation in HeLa cells, an effect depending on its kinase activity. HeLa cells were transfected with control EGFP (EGFP/Ctrl), EGFP/MRCKβ full-length (FL), EGFP/MRCKβ kinase domain (1–430), or EGFP/MRCKβ kinase-inactive K105M mutant plasmids. After 48 h, cells were fixed and stained with fluorescent dye conjugated phalloidin to show actin filaments. EGFP fluorescence was used to show transfected cells. Scale bar, 7.5 μm. *B*, stress fiber formation was quantified by measuring stress fiber numbers per cell. Results were expressed as mean ± SD; n = 10 to 11; $^{**}p < 0.01$, n.s., not significant; Ordinary one-way ANOVA (F (3, 42) = 20.40, $p < 0.0001$). *C*, Dasm1 promoted stress fiber formation in HeLa cells, an effect depending on intracellular MRCKβ-binding PRR domain but not on extracellular region. HeLa cells were transfected with control EGFP (EGFP-Ctrl), EGFP-Dasm1 full-length plasmid (FL), EGFP-Dasm1 1 to 974 truncate (containing intracellular MRCKβ-binding PRR domain), EGFP-Dasm1 PRR deletion mutant (Dasm1ΔPRR), or EGFP-Dasm1 1 to 718 truncate (extracellular region). After 48 h, transfected cells were fixed and stained with antiphalloidin antibody to show actin filaments. EGFP fluorescence was used to show transfected cells. Scale bar, 7.5 μm. *D*, stress fiber formation was quantified by measuring stress fiber number per cell. Results were expressed as mean ± SD; n = 12 to 16; $^{**}p < 0.01$, n.s., not significant; Ordinary one-way ANOVA (F (4, 59) = 79.15, $p < 0.0001$). MRCKβ, myotonic dystrophy-related Cdc42-binding kinases beta; PRR, proline-rich region.

consequence of reduced synaptic inhibition (38). Interestingly, Mishra *et al.* observed that both *Dasm1* RNAi constructs, and its dominant negative construct can reduce dendrite complexity as we reported previously (7). While they attributed the former to off-target effects and could not explain the latter (37). In current study, we verified that RNAi constructs-caused phenotypes were rescued by RNAi-resistant Dasm1 full-length cDNA, but not by Dasm1 wild-type cDNA, which demonstrated that these phenotypes were not due to off-target effects (Fig. S1, *A–C*). Meanwhile, we found a decreased total dendrite length and branches in early postnatal life (P5, P15, and P30) but not in the late postnatal life (P60) in *Dasm1*$^{-/-}$ mice. Correspondingly, adolescent, but not adult *Dasm1*$^{-/-}$ mice showed learning or memory defects and anxiety/

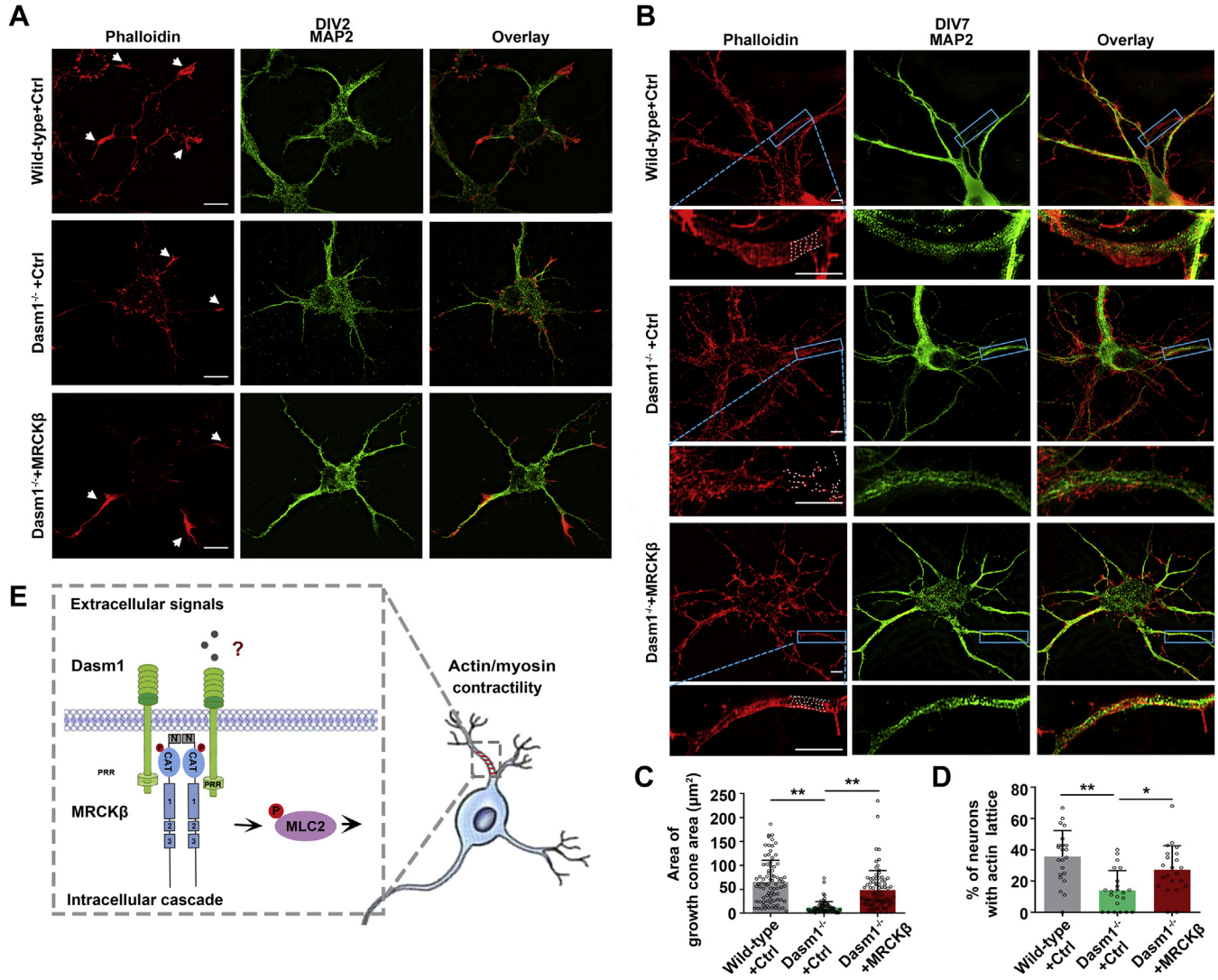

Figure 7. MRCKβ rescues actin cytoskeleton disruption caused by Dasm1 deficiency. *A*, representative images of 2 DIV primary hippocampal neurons using N-structured illumination microscopy (N-SIM) super-resolution microscopy. Primary hippocampal neurons from *Dasm1*$^{-/-}$ mice were transfected with control (Ctrl) or MRCKβ plasmid at 0 DIV, cultured for 2 days, and then stained with phalloidin (*red*, F-actin marker), and MAP2 (*green*, dendrite marker). *White arrows* indicated growth cones. Scale bars, 10 μm. *B*, representative images of 7 DIV primary hippocampal neurons using N-SIM super-resolution microscopy. Primary hippocampal neurons from *Dasm1*$^{-/-}$ mice were transfected with control (Ctrl) or MRCKβ plasmid at 3 DIV, cultured for 4 days, and then stained with Phalloidin (*red*) and MAP2 (*green*). Scale bar, 10 μm. Corresponding *lower panel*: intensity profile corresponding to *dashed line* in box of *upper panel*. *Dashed line* indicated periodic actin lattice. Scale bar, 2.5 μm. *C*, MRCKβ rescued the decreased growth cone area in dendrites of *Dasm1*$^{-/-}$ neurons. Results were expressed as mean ± SD; n = 81; $^{**}p < 0.01$; Kruskal-Wallis test (F (2, 240) = 47.29, $p < 0.0001$). *D*, MRCKβ rescued the decreased percentage of actin periodicity in dendrites of *Dasm1*$^{-/-}$ neurons. Results were expressed as mean ± SD; n = 22; $^{*}p < 0.05$, $^{**}p < 0.01$; Ordinary one-way ANOVA (F (2, 63) = 11.52, $p < 0.0001$). *E*, the proposed model depicts the role of Dasm1 in dendrite development. Dasm1 transmits an as-yet-unknown stimulus to interior of cells by interacting with MRCKβ kinase CC1 domain *via* its PRR region. Consequently, MRCKβ autoinhibitory loop is opened and allows its dimerization and autophosphorylation. In turn, MRCKβ kinase is activated and leads to the phosphorylation of downstream substrate MLC2 and consequent increased actin/myosin contractility, which promotes dendrite morphogenesis. DIV, day *in vitro*; MRCKβ, myotonic dystrophy-related Cdc42-binding kinases beta; PRR, proline-rich region.

depression-like phenotype, which suggest Dasm1 may function in a developmental stage-dependent manner. Together, these results demonstrated that Dasm1 ensured a proper dendritic development, including the dendritic arbor and spine formation, both *in vitro* and *in vivo*.

Dendrites and spines structures receive input from other neurons or glial cells and determine how signals integrated (1). The morphological modifications of dendrites spines are widely regarded as the structural basis for learning, encoding memories, and emotional process. Abnormal development of dendritic morphology and spines formation are common findings in many aging-related behavior (learning and memory defects *et al.*), neurodevelopmental disorders (schizophrenia, Down's syndrome, fragile X syndrome, and autism *et al.*), and neurodegenerative (Alzheimer's disease, and prion diseases *et al.*) pathologies (39–42), which lead to cognitive and emotional behavioral abnormalities. For example, disruption of Prickle2, a noncanonical Wnt signaling protein, led to reductions in dendrite branching and outgrowth in hippocampal neurons (43). Prickle2 malfunction mice display ASD-like phenotypes including altered social interaction, and learning abnormalities (43). DSCAM, a number of Ig cell adhesion

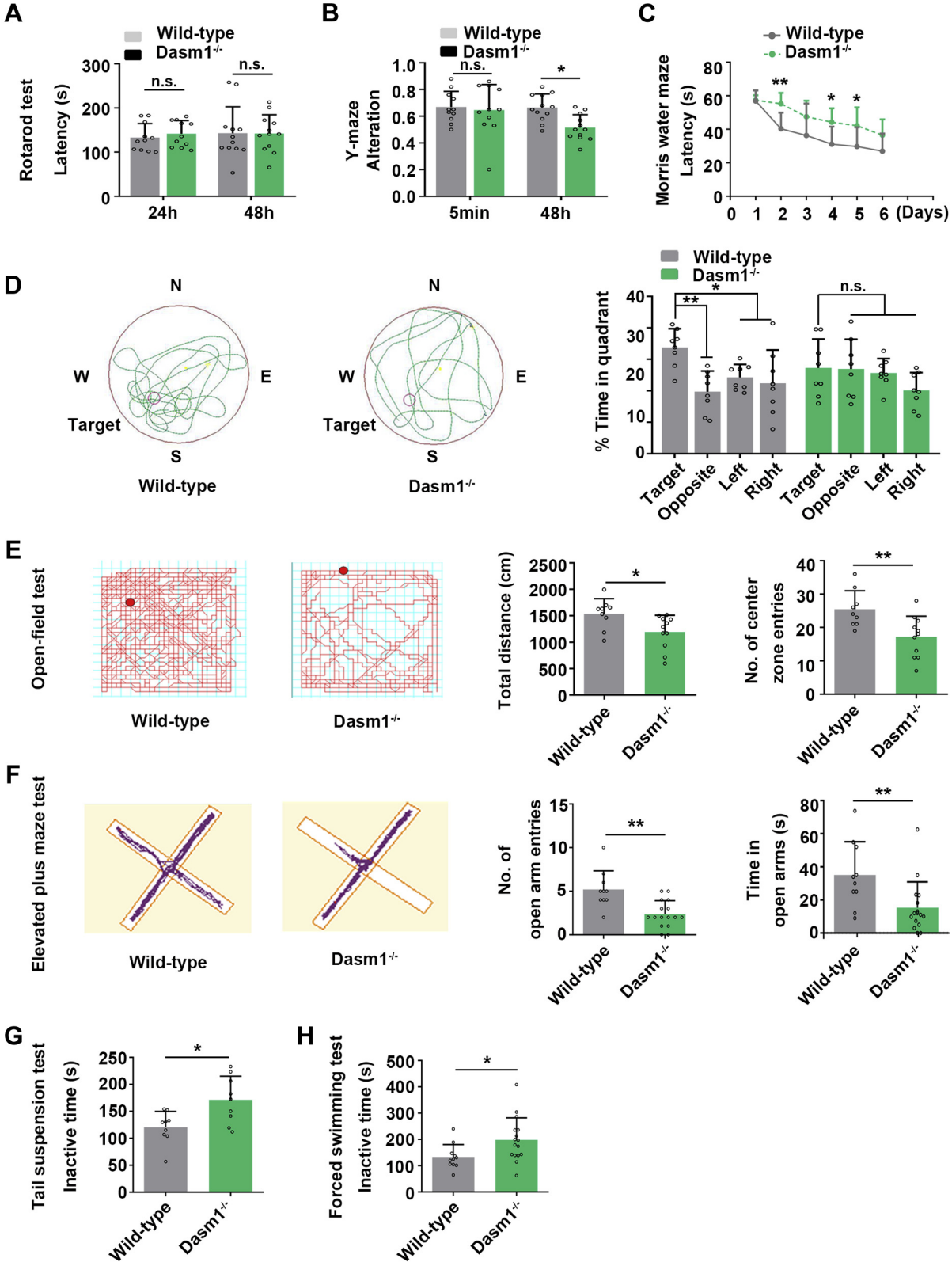

Figure 8. Adolescent Dasm1 knockout mice exhibit defective learning and memory abilities, accompanied by mood disorders. *A*, motor coordination and balance ability were normal in adolescent (5 weeks) *Dasm1*$^{-/-}$ mice. Rotarod test showed no difference in latency time between adolescent *Dasm1*$^{-/-}$ mice and WT littermates. Results were expressed as mean ± SD; n = 11 to 12; n.s., not significant; two-way ANOVA (Interaction: F (1, 42) = 0.1327, p = 0.7175; Row Factor: F (1, 42) = 0.1659, p = 0.6859; Column factor: F (1, 42) = 0.09277, p = 0.7622). *B*, adolescent *Dasm1*$^{-/-}$ mice exhibited a defective working memory in Y-maze test. The spontaneous alternation of adolescent *Dasm1*$^{-/-}$ mice significantly decreased compared with adolescent WT littermates. Results were expressed as mean ± SD; n = 10 to 11; *$p < 0.05$, n.s., not significant; two-way ANOVA (Interaction: F (1, 42) = 2.709, p = 0.1073; Row Factor: F (1, 42) = 3.144, p = 0.0835; Column factor: F (1, 42) = 4.989, p = 0.0309). *C* and *D*, adolescent *Dasm1*$^{-/-}$ mice exhibited defective spatial learning and memory in Mirror water maze test. *C*, in training phase, adolescent *Dasm1*$^{-/-}$ mice took a longer time to reach the hidden platform than adolescent WT

molecules, regulates pyramidal dendrite arborization and spine formation during circuit development (44). Mice bearing the spontaneous mutation DSCAMdel17 show depression and anxiety disorders (45). In our study, *Dasm1*$^{-/-}$ mice showed reduced dendrite arborization and spine density, which may explain its learning/memory defects and anxiety/depression-like phenotype. Moreover, Dasm1 dysfunction increased the proportion of immature thin spines and decreased the proportion of mature mushroom spines *in vitro* and *in vivo* (Fig. 1*J* and Fig. S2*J*), indicating a decreased spine maturation. It is consistent with the findings that aging and related disease declines in cognitive ability are accompanied by decreases in spine maturation (22, 40).

There was a phenotypic difference between the adult and the adolescent *Dasm1*$^{-/-}$ mice in the present study. Adult *Dasm1*$^{-/-}$ mice showed no learning or memory defects or anxiety/depression-like phenotype. This difference might be because of the lack of expression of Dasm1 during late-stage development and the possible compensatory effect of another IgSF9 family protein, IgSF9b. Supportively, we found that the expression of Dasm1 gradually decreased over time and was almost undetectable in 2-month-old mice, whereas the expression of IgSF9b, a Dasm1 homologous protein, gradually increased with age and reached a peak at 2 months (Fig. S8*A*). IgSF9b shared high module-to-module similarity with Dasm1, with their Ig domains and fibronectin III domains exhibiting 51% and 45% identity, respectively (32). Whether IgSF9b shared the similar function with Dasm1? We found that overexpression of IgSF9b can rescue the defects in dendrite arborization at 6DIV and 10DIV in cultured primary hippocampal neurons (Fig. S8, *B–D*). Likely, the recovery of both cellular and behavioral deficits in adults might reflect the delayed expression of IgSF9b.

Collectively, our results indicated that Dasm1, coupled with MRCKβ signaling, regulates the actin cytoskeleton, dendritic morphogenesis, and spine formation.

Experimental procedures

Generation of Dasm1 knockout mice

Dasm1 knockout mice were generated by homologous recombination in embryonic stem cells (46). A 6.5 kb genomic fragment (containing exons 7–20 of Dasm1 gene) was amplified from 129SVJ mouse DNA by PCR and was used to construct the Dasm1 targeting vector. The 4.1-kb and 2.2-kb fragments were inserted separately as long and short homology arms, respectively, into a modified pL451 vector. The targeting vector was linearized with NotI and electroporated into 129SVJ mouse embryonic stem cells. G418-resistant colonies were picked, expanded, and screened for homologous recombination by Southern blot. Homologous recombinant ES cells were injected into C57Bl/6 blastocysts, and chimeric male mice were obtained which were mated to C57Bl/6 females to establish a mouse line carrying the Dasm1-neo allele. Dasm1 knockout mice were genotyped routinely by isolating genomic tail DNA and performing PCR with the following primers: p1S (neo): 5′-TGCTCCTGCCGA-GAAAGTATCCATCATGGC-3′ and p1AS (neo): 5′-CGCCAAGCTCTTCAGCAATATCACGGGTAG-3′; p2S (pGKb): 5′-CTAAAGCGCATGCTCCAGACT-3′ and p2AS (pGKb): 5′-TGCAAAT GGGCTCTAATGGTAAGGGTC-3′; p3S (Dasm1): 5′-GTCCCCAGCTCCGTGC GGACAGAA-TAG-3′ and p3AS (Dasm1): 5′-GAGGTG AAAATGGC-CAAGTCAG GATGAGAA-3′. The 586 bp WT, 380 bp, or 1.4 kb Dasm1 targeted allele bands were resolved on 1.5% agarose gels. All animals were group-housed under normal light-dark cycle with food and water *ad libitum*. All animal experimental protocols were preapproved by the Ethics Committee of Experimental Animals of Fudan University in accordance with Institutional Animal Care and Use Committee guidelines for animal research.

Cell culture and plasmids construction

HEK293T and HeLa cells were cultured in DMEM/high-glucose medium (Thermo Fisher Scientific) supplemented with 10% fetal bovine serum (Thermo Fisher Scientific), 1% penicillin, and streptomycin (Thermo Fisher Scientific) at 37 °C, in a humidified atmosphere containing 5% CO_2. cDNA constructs were cloned into pIRES-EGFP (Thermo Fisher Scientific) for imaging studies, pCMV-Tag2B (Agilent Stratagene) and pcDNA3.1 (Thermo Fisher Scientific) for overexpression of wild-type and mutants' proteins, and pEGX-KG (ATCC) for GST pull-down assays. The U6 promoter and shRNA sequence were cloned into pIRES-EGFP vector to construct nonfused recombinant plasmids: EGFP/*Dasm1*-sh/WT, EGFP/*Dasm1*-sh/Rescue, EGFP/*Dasm1*-sh/*MRCKβ* FL, EGFP/*Dasm1*-sh/*MRCKβ* 1 to 430 and EGFP/*Dasm1*-sh/*MRCKβ* FL ^{K105M}. The *Dasm1* shRNA sequence used in this study was described in our previous study (shRNA: 5' GCCTGAGGTGGTCTCTGTG 3') (7, 8). Deletion and site-directed mutations were incorporated into plasmid DNA

littermates. Results were expressed as mean ± SD; n = 8; $^{**}p < 0.01$; Unpaired two-tailed *t* test. *D*, in testing phase, adolescent *Dasm1*$^{-/-}$ mice showed no spatial preference, while adolescent WT littermates showed a prominent preference for target quadrant. *Left panel*, representative exploratory tracks in water maze without hidden platform. *Right panel*, quantification of the time which mice spent in target quadrant and other quadrants. Results were expressed as mean ± SD; n = 8; $^{*}p < 0.05$, $^{**}p < 0.01$, n.s., not significant; two-way ANOVA (Interaction: F (3, 56) = 2.486, $p = 0.0699$; Row Factor: F (3, 56) = 4.647, $p = 0.0057$; Column factor: F (1, 56) = 0.0004460, $p = 0.9832$). *E*, adolescent *Dasm1*$^{-/-}$ mice were less active in the open-field test than WT littermates. *Left panel*, representative exploratory tracks in the open field. *Middle panel*, adolescent *Dasm1*$^{-/-}$ mice exhibited shorter moving distance in open field than adolescent wild-type littermates. *Right panel*, adolescent *Dasm1*$^{-/-}$ mice exhibited fewer entries into the center zone of open field than adolescent WT littermates. Results were expressed as mean ± SD; n = 9 to 11; $^{*}p < 0.05$, $^{**}p < 0.01$; Unpaired two-tailed *t* test. *F*, adolescent *Dasm1*$^{-/-}$ mice were less active in elevated plus maze than adolescent WT littermates. *Left panel*, representative exploratory tracks in elevated plus maze. *Middle panel*, adolescent *Dasm1*$^{-/-}$ mice had fewer entries into open arms than adolescent WT littermates. *Right panel*, adolescent *Dasm1*$^{-/-}$ mice spent less time in open arms than adolescent WT littermates. Results were expressed as mean ± SD; n =10 to 16; $^{**}p < 0.01$; Unpaired two-tailed *t* test or Mann-Whitney two-tailed test. *G* and *H*, adolescent *Dasm1*$^{-/-}$ mice exhibited depression-like behavior. Adolescent *Dasm1*$^{-/-}$ mice displayed longer inactive time in Tail Suspension Test (*G*) and Forced Swimming Test than adolescent WT littermates (*H*). Results were expressed as mean ± SD; n = 9 to 16; $^{*}p < 0.05$; unpaired two-tailed *t* test.

using Q5 Site-Directed Mutagenesis kit (New England Biolabs). All primers used in this study were listed in Table S1.

Hippocampal neuron culture, transfection, and immunofluorescence assay

The hippocampal neuron culture was performed as previously described (47). For dissociated hippocampal neuronal cultures, we used E14 embryo from the pregnant female mice. The hippocampus was dissected from the mice at embryonic day 14 and dissociated with enzyme solution at 37 °C for 15 min. After centrifugation, hippocampal cells were suspended in plating medium and inoculated in 24-well plates; the medium was then replaced with maintenance medium. To maintain neurons, half of the maintenance medium was aspirated and replaced with fresh medium twice a week. Neurons were cultured for 3 DIV and transfected with Lipofectamine 3000 (Thermo Fisher Scientific). Neurons were fixed at 6 DIV, 10 DIV, or 25 DIV with 4% paraformaldehyde at 4 °C for 30 min. The fixed neurons were permeabilized with 0.3% Triton X-100 in PBS for 10 min and blocked with 10% horse serum in PBS at room temperature for 1 h. Neurons were then incubated with the primary antibody at 4 °C overnight, incubated with secondary antibodies at room temperature for 2 h, and then covered for microscopy. The antibodies and dilutions used were listed in Table S2.

Golgi staining

Golgi staining was performed using the FD Rapid GolgiStain Kit (FD NeuroTechnologies). Mouse brain tissues were dissected and immersed in a premixed reagent with equal volumes of Golgi solutions A and B for 2 weeks in the dark. The tissue was then transferred to solution C and stored in the dark for at least 72 h at room temperature. After incubation, tissues were embedded in OCT (Sakura) and cut into sections (100–200 μm) at −20 °C. Brain sections were placed in a staining solution consisting of Solution D, Solution E, and double distilled water (1:1:2) for 10 min. The slides were then dehydrated in 50%, 75%, and 95% ethanol, washed in xylene, and then covered with Permount Mounting Medium for microscopy.

Yeast two-hybrid screening

Yeast two-hybrid screen was performed as described previously (8). The bait plasmid expressing the PRR domain of *Dasm1* fused with *Gal4* DNA-binding domain in pPC97 vector was used to screen a rat brain cDNA library fused to *Gal4* transcriptional activation domain in pPC86 vector. Positive clones were selected on quadruple minus plates (Leu-, Try-, Ade-, and His-) and blue assays (48). All cDNAs from positive clones were recovered and back-transformed to confirm the interaction.

Western blot

Total protein was extracted from cells and tissues in RIPA lysis buffer and separated in sodium dodecyl sulfate-polyacrylamide gel electrophoresis before electrotransferred onto polyvinylidene difluoride membrane (Merck Millipore) as previously described (49). After blocked with 3% BSA for 1 h at room temperature, the membrane was incubated with primary antibody overnight at 4 °C. Subsequently, the membrane was incubated with a secondary antibody for 1.5 h at room temperature. The antibodies and dilutions used were listed in Table S2. Immunoreactive bands on the membrane were visualized by the enhanced chemiluminescence assay.

Co-immunoprecipitations

For immunoprecipitation of overexpressed proteins, HEK293T cells were transfected with specific cDNA constructs (50). Cell lysates were precleared with protein A/G beads (Santa Cruz) for 3 h. The cleared supernatants were incubated with protein A/G beads and a specific antibody at 4 °C for 16 h. After washing with lysis buffer three times, the immunoprecipitates were detected by western blotting. For immunoprecipitation of tissues, the hippocampus was dissected from C57BL/6 mice and lysed and then processed similarly using specific antibodies. The antibodies and dilutions used were listed in Table S2.

GST pull-down assay

GST pull-down assay was performed as previously described (50). GST, GST-Dasm1 PRR, GST-MRCKβ CC1, and GST-MRCKβ 1 to 939 fusion proteins were expressed in bacterial BL21. Bacterial cells were lysed, and GST fusion proteins were captured using Glutathione-Sepharose 4B beads (GE Healthcare Life Sciences) at 4 °C for 1 h. To investigate the interaction between Dasm1 and MRCKβ, GST or GST-Dasm1 PRR fusion protein beads were incubated with *in vitro*-translated MRCKβ in equal amounts. GST, GST-MRCKβ CC1, or GST-MRCKβ 1 to 939 fusion protein beads were incubated with *in vitro*-translated Dasm1. After washing with ice-cold wash buffer, the proteins were eluted from the beads and detected by Western blotting.

In vitro *immunoprecipitation and kinase assay*

The GST-MLC2 fusion protein was expressed in BL21 bacterial cells and purified using Glutathione-Sepharose 4B beads. HEK293T cells were transfected with constructs of HA-MRCKβ alone or co-transfected with HA-MRCKβ and Myc-Dasm1. Expressed proteins were immunoprecipitated with anti-HA antibody, and the recovered immunoprecipitants were assayed for MRCKβ kinase activity. The kinase assay was carried out at 30 °C for 30 min using GST-MLC2 as the substrate in the buffer containing 10 μM ATP, 25 mM MOPS, pH7.2, 12.5 mM β-glycerophosphate, 25 mM MgCl2, 5 mM EGTA, 2 mM EDTA, and 0.25 mM DTT (21).

Autophosphorylation assay

HeLa cells were transfected with constructs of HA-*MRCKβ* alone or co-transfected with HA-*MRCKβ* and Myc-*Dasm1*. Expressed proteins were immunoprecipitated with anti-HA antibody. The recovered immunoprecipitants were then employed for MRCKβ autophosphorylation assays.

Autophosphorylation assays were carried out at 30 °C for 30 min in buffer containing 10 μM [γ-33P] ATP (2500 Ci/mmol; NEN), 25 mM MOPS, pH7.2, 12.5 mM β-glycerolphosphate, 25 mM $MgCl_2$, 5 mM EGTA, and 2 mM EDTA, 0.25 mM DTT (20).

BS^3 cross-linking assay

Total protein was extracted from HeLa cells in IP lysis buffer. For BS^3 cross-linking reaction, 0.05 to 0.25 mM bis (sulfosuccinimidyl) suberate (BS^3; Pierce Thermo Fisher Scientific) was added at 4 °C for 30 min, then the reaction was quenched with SDS-PAGE sample buffer. The cross-linked products were detected by Western blot (20).

The structural analysis of MRCKβ/Dasm1 complex

The three-dimensional structures of Dasm1 (759–974 aa) and MRCKβ (1–744 aa) were carried out with I-TASSER, FRt5-M, and FALCON software (51, 52). The candidate interfaces which involved in protein–protein interaction were selected with ISPRED4 (53). According to the candidate interfaces, MRCKβ and Dasm1 complexes were docked with HDOCK (54), and the highest-confidence complex model was selected from ten candidate models using HDOCK and SPR score (55). And the amino acid residues with spatial distance less than 3 Å between the residues of MRCKβ and Dasm1 were identified. All structure models were shown by PyMol Software (www.pymol.org).

Behavioral test

To eliminate the interference of hormones, we chose male mice for behavioral experiments. All animals were group-housed under normal light-dark cycle with food and water *ad libitum*.

Rotarod

Motor coordination and balance were measured using a commercially available accelerating rotarod apparatus (Med Associates). Mice were placed on the rotating cylinder (diameter, 7 cm). And the rotarod accelerated from 4 to 40 rpm over the course of a 5 min trial. Mice were tested for three trials per day for two consecutive days (0 h, 24 h, and 48 h). The mice rested in their home cages for 20 min between each trial. The latency of fall or stop time was recorded as a parameter for motor coordination and balance.

Y-maze test

The Y-maze was performed as previously described (56). Y-maze was measured in the three-armed apparatus, with an angle of 120° between each arm labeled as A, B, and C. The mice were placed in the center of the maze and allowed to move freely for 6 min, and the number of arm entries and alternations are recorded to calculate the percentage of the alternation behavior. After a certain time interval (5 min and 48 h), the mice were placed back into the maze to examine short-term (5 min) and long-time working memory (48 h), respectively. The sequence and total number of arms entered were recorded. An alternation is defined as the mouse entering all three arms consecutively. The percent (%) alternation was calculated using the following formula: (%) Alternation = Number of Alternations/(Total number of arm entries -2)*100

Morris water maze test

Morris water maze test was performed for seven consecutive days and consisted of a 6-days training trail and a 1-day testing trial as previously described (57). During the training days, mice were placed in the pool filled with water at approximately 23 to 25 °C. Each mouse received one blocks of testing per day; each block was composed of four sequential trials. For each trial, the mouse was placed into the pool at a different start location and was allowed to find the hidden platform within 1 min. Once found the platform within 1 min, the mouse was allowed to stay on the platform for 15 s. If not, the mice would be guided to the platform and remain for 30 s. At the testing day, the platform was removed, and the mice were placed in pool from a new site. The latency time (meaning the duration to reach the platform), exploratory tracks, and time spent in the platform quadrant were recorded to analyze the mice ability of learning and memory.

Open-field test

Open-field test was performed in an open field chamber under dim light (length, 40 cm; width, 40 cm; height, 30 cm) (Med Associates) (58). Mice were gently placed in the center of the chamber and allowed to move freely for 8 min. The EthoVision XT 8.5 tracking software (Noldus) was used to analyze exploratory tracks and time in the center zones (inner 25% of the surface area, away from the walls).

Elevated plus maze test

Elevated plus maze test was performed in an apparatus which consisted of two closed arms (width, 6 cm; length, 35 cm; and high walls, 20 cm) and two open arms (width, 6 cm; length, 35 cm; without wall) elevated 50 cm above the floor (Med Associates). Mice were placed at the intersection of four arms and allowed to move freely for 5 min. The entries number and the time spent in the open or closed arms were recorded as a parameter for anxiety.

Tail suspension test

The tail suspension test was performed on the basis of previous method (59). Mice were hung 15 cm above the floor by the tip of the tail (1 cm) and adhered to an aluminum bar. Mice were suspended for 6 min, and their behavior was videotaped. Their activities was recorded, and the inactive frequency was analyzed as a parameter for depression. The inactive frequency was defined as the change frequency of mice from mobility to immobility within 6 min.

Forced swimming test

Forced swimming test was performed in a plastic cylinder (height, 15 cm; diameter, 11 cm) containing water (30 cm depth) at approximately 23 to 25 cm (60). Mice were placed into the cylinder for 6 min, and their behavior was videotaped. The inactive time was recorded as a parameter for depression. The inactive stage was defined as the mouse not making any active movements other than those necessary to keep the head and nose above the water. The animals were dried immediately and returned to their home cages after the test.

Image analysis

For all morphological analyses, dendritic branches were traced using the NeuronJ plugin in Fiji/ImageJ (NIH), and dendritic length was measured using the ImageJ. Sholl analysis was performed with Fiji/ImageJ, in which concentric circles with a 20 μm spacing were drawn around the cell body, and the intersection number of all dendritic branches with the circles was counted. Spine number, spine length, and spine width were semiautomatically measured using ImageProPlus (Media Cybernetics). Spine subtypes were classified based on previously defined morphological criteria (61) and quantitated as follows: Thin spine: diameters of spine head and neck are nearly equal, and spine length is greater than spine width ($d_h/d_n < 1.5$, $L/d_h \geq 1.5$); Mushroom spine: the spine head diameter is greater than or equal to 1.5 times of neck diameter ($d_h/d_n \geq$ d.5 M); Stubby spine: head and neck of the spine are approximately of same width, and spine length is not significantly longer than the head diameter ($d_h/d_n < 1.5$, $L/d_h < 2$); Branched spine: spines with more than one head. The quantifications were done independently by three experienced technicians blinded to the knowledge of control and test group.

Statistical analysis

All data were analyzed statistically using GraphPad Prism, Version 7.0. All results were presented as mean ± SD. Shapiro-Wilk test was performed to check the data distribution. Unpaired two-tailed *t* test or Mann Whitney two-tailed test was used for comparison between two groups. Ordinary one-way ANOVA with Dunnett's post hoc or Kruskal-Wallis test followed by Dunn's post hoc according to the Gaussian or non-Gaussian distribution of the data was used for comparison among multiple groups. For two independent variables, ordinary two-way ANOVA with Bonferroni post hoc was carried out. A value $p < 0.05$ (two-side) was considered statistically significant.

Data availability

All data described in this manuscript are available in the main text or supporting information.

Supporting information—This article contains supporting information.

Acknowledgments—We greatly appreciate Professor Mingjie Zhang from Hong Kong University of Science and Technology for providing MRCKβ cDNAs, Professor Ivan Tan from National University of Singapore for providing MRCKα cDNAs. This work was supported by grants from the National Natural Science Foundation of China (81772615, 81573423, and 81770137).

Author contributions—S. C., S.-H. S., Z.-Q. Y., and S. Z. designed and conceived this project. S. C. and X.-X. W. developed methodology. S. Z., X.-X. W., P.-P. D., Y.-H. L., and L. Z. performed experiments and generated data. S. Z., X.-X. W., P.-P. D., and Z.-Q. Y. analyzed and interpreted data. S. Z. and X.-X. W. wrote the draft. S. C. and S.-H. S. revised and finalized the manuscript. All authors contributed to and approved the manuscript.

Conflict of interest—The authors declare that they have no conflicts of interest with the contents of this article.

Abbreviations—The abbreviations used are: DIV, day *in vitro*; IgSF, immunoglobulin superfamily; MLC2, class 2 regulatory myosin light chains; MRCKβ, myotonic dystrophy-related Cdc42-binding kinases beta; PRR, proline-rich region.

References

1. Berry, K. P., and Nedivi, E. (2017) Spine dynamics: Are they all the same? *Neuron* **96**, 43–55
2. Magee, J. C. (2000) Dendritic integration of excitatory synaptic input. *Nat. Rev. Neurosci.* **1**, 181–190
3. Koleske, A. J. (2013) Molecular mechanisms of dendrite stability. *Nat. Rev. Neurosci.* **14**, 536–550
4. Jan, Y., and Jan, L. Y. (2010) Branching out: Mechanisms of dendritic arborization. *Nat. Rev. Neurosci.* **11**, 316–328
5. Forrest, M. P., Parnell, E., and Penzes, P. (2018) Dendritic structural plasticity and neuropsychiatric disease. *Nat. Rev. Neurosci.* **19**, 215–234
6. Sytnyk, V., Leshchyns'Ka, I., and Schachner, M. (2017) Neural cell adhesion molecules of the immunoglobulin superfamily regulate synapse formation, maintenance, and function. *Trends. Neurosci.* **40**, 295–308
7. Shi, S. H., Cox, D. N., Wang, D., Jan, L. Y., and Jan, Y. N. (2004) Control of dendrite arborization by an Ig family member, dendrite arborization and synapse maturation 1 (Dasm1). *Proc. Natl. Acad. Sci. U. S. A.* **101**, 13341–13345
8. Shi, S. H., Cheng, T., Jan, L. Y., and Jan, Y. N. (2004) The immunoglobulin family member dendrite arborization and synapse maturation 1 (Dasm1) controls excitatory synapse maturation. *Proc. Natl. Acad. Sci. U. S. A.* **101**, 13346–13351
9. He, H. J., Wang, X. S., Pan, R., Wang, D. L., Liu, M. N., and He, R. Q. (2009) The proline-rich domain of tau plays a role in interactions with actin. *BMC Cell Biol.* **10**, 81
10. Holt, M. R., and Koffer, A. (2001) Cell motility: Proline-rich proteins promote protrusions. *Trends. Cell Biol.* **11**, 38–46
11. Pak, C. W., Flynn, K. C., and Bamburg, J. R. (2008) Actin-binding proteins take the reins in growth cones. *Nat. Rev. Neurosci.* **9**, 136–147
12. Lowery, L. A., and Van Vactor, D. (2009) The trip of the tip: Understanding the growth cone machinery. *Nat. Rev. Mol. Cell Biol.* **10**, 332–343
13. Konietzny, A., Bar, J., and Mikhaylova, M. (2017) Dendritic actin cytoskeleton: Structure, functions, and regulations. *Front. Cell Neurosci.* **11**, 147
14. D'Este, E., Kamin, D., Gottfert, F., El-Hady, A., and Hell, S. W. (2015) STED nanoscopy reveals the ubiquity of subcortical cytoskeleton periodicity in living neurons. *Cell Rep.* **10**, 1246–1251
15. Han, B., Zhou, R., Xia, C., and Zhuang, X. (2017) Structural organization of the actin-spectrin-based membrane skeleton in dendrites and soma of neurons. *Proc. Natl. Acad. Sci. U. S. A.* **114**, E6678–E6685

16. Xu, K., Zhong, G., and Zhuang, X. (2013) Actin, spectrin, and associated proteins form a periodic cytoskeletal structure in axons. *Science* **339**, 452–456
17. Leung, T., Chen, X. Q., Tan, I., Manser, E., and Lim, L. (1998) Myotonic dystrophy kinase-related Cdc42-binding kinase acts as a Cdc42 effector in promoting cytoskeletal reorganization. *Mol. Cell. Biol.* **18**, 130–140
18. Falls, D. L. (2005) Dasm1: A receptor that shapes neuronal dendrites and turns on silent synapses? *Sci. STKE* **2005**, e10
19. Unbekandt, M., and Olson, M. F. (2014) The actin-myosin regulatory MRCK kinases: Regulation, biological functions and associations with human cancer. *J. Mol. Med. (Berl.)* **92**, 217–225
20. Tan, I., Seow, K. T., Lim, L., and Leung, T. (2001) Intermolecular and intramolecular interactions regulate catalytic activity of myotonic dystrophy kinase-related Cdc42-binding kinase alpha. *Mol. Cell. Biol.* **21**, 2767–2778
21. Tan, I., Yong, J., Dong, J. M., Lim, L., and Leung, T. (2008) A tripartite complex containing MRCK modulates lamellar actomyosin retrograde flow. *Cell* **135**, 123–136
22. Martinez-Cerdeno, V. (2017) Dendrite and spine modifications in autism and related neurodevelopmental disorders in patients and animal models. *Dev. Neurobiol.* **77**, 393–404
23. Choi, S. H., Czifra, G., Kedei, N., Lewin, N. E., Lazar, J., Pu, Y., Marquez, V. E., and Blumberg, P. M. (2008) Characterization of the interaction of phorbol esters with the C1 domain of MRCK (myotonic dystrophy kinase-related Cdc42 binding kinase) alpha/beta. *J. Biol. Chem.* **283**, 10543–10549
24. Arabzadeh, A., and Quail, D. F. (2019) Myosin II in cancer cells shapes the immune microenvironment. *Trends. Mol. Med.* **25**, 257–259
25. Huo, L., Wen, W., Wang, R., Kam, C., Xia, J., Feng, W., and Zhang, M. (2011) Cdc42-dependent formation of the ZO-1/MRCKbeta complex at the leading edge controls cell migration. *EMBO J.* **30**, 665–678
26. Birch, J. L., Strathdee, K., Gilmour, L., Vallatos, A., McDonald, L., Kouzeli, A., Vasan, R., Qaisi, A. H., Croft, D. R., Crighton, D., Gill, K., Gray, C. H., Konczal, J., Mezna, M., McArthur, D., *et al.* (2018) A novel small-molecule inhibitor of MRCK prevents radiation-driven invasion in glioblastoma. *Cancer Res.* **78**, 6509–6522
27. Unbekandt, M., Belshaw, S., Bower, J., Clarke, M., Cordes, J., Crighton, D., Croft, D. R., Drysdale, M. J., Garnett, M. J., Gill, K., Gray, C., Greenhalgh, D. A., Hall, J., Konczal, J., Lilla, S., *et al.* (2018) Discovery of potent and selective MRCK inhibitors with therapeutic effect on skin cancer. *Cancer Res.* **78**, 2096–2114
28. Zihni, C., Vlassaks, E., Terry, S., Carlton, J., Leung, T. K. C., Olson, M., Pichaud, F., Balda, M. S., and Matter, K. (2017) An apical MRCK-driven morphogenetic pathway controls epithelial polarity. *Nat. Cell Biol.* **19**, 1049–1060
29. Scott, E. K., Reuter, J. E., and Luo, L. (2003) Small GTPase Cdc42 is required for multiple aspects of dendritic morphogenesis. *J. Neurosci.* **23**, 3118–3123
30. Rex, C. S., Gavin, C. F., Rubio, M. D., Kramar, E. A., Chen, L. Y., Jia, Y., Huganir, R. L., Muzyczka, N., Gall, C. M., Miller, C. A., Lynch, G., and Rumbaugh, G. (2010) Myosin IIb regulates actin dynamics during synaptic plasticity and memory formation. *Neuron* **67**, 603–617
31. Hering, H., and Sheng, M. (2001) Dendritic spines: Structure, dynamics and regulation. *Nat. Rev. Neurosci.* **2**, 880–888
32. Hansen, M., and Walmod, P. S. (2013) IGSF9 family proteins. *Neurochem. Res.* **38**, 1236–1251
33. Long, H., Ou, Y., Rao, Y., and van Meyel, D. J. (2009) Dendrite branching and self-avoidance are controlled by turtle, a conserved IgSF protein in Drosophila. *Development* **136**, 3475–3484
34. Ferguson, K., Long, H., Cameron, S., Chang, W. T., and Rao, Y. (2009) The conserved Ig superfamily member turtle mediates axonal tiling in Drosophila. *J. Neurosci.* **29**, 14151–14159
35. Al-Anzi, B., and Wyman, R. J. (2009) The Drosophila immunoglobulin gene turtle encodes guidance molecules involved in axon pathfinding. *Neural Dev.* **4**, 31
36. Sulkowski, M. J., Iyer, S. C., Kurosawa, M. S., Iyer, E. P., and Cox, D. N. (2011) Turtle functions downstream of cut in differentially regulating class specific dendrite morphogenesis in Drosophila. *PLoS One* **6**, e22611
37. Mishra, A., Knerr, B., Paixao, S., Kramer, E. R., and Klein, R. (2008) The protein dendrite arborization and synapse maturation 1 (Dasm-1) is dispensable for dendrite arborization. *Mol. Cell. Biol.* **28**, 2782–2791
38. Mishra, A., Traut, M. H., Becker, L., Klopstock, T., Stein, V., and Klein, R. (2014) Genetic evidence for the adhesion protein IgSF9/Dasm1 to regulate inhibitory synapse development independent of its intracellular domain. *J. Neurosci.* **34**, 4187–4199
39. Galvez, R., Gopal, A. R., and Greenough, W. T. (2003) Somatosensory cortical barrel dendritic abnormalities in a mouse model of the fragile X mental retardation syndrome. *Brain Res.* **971**, 83–89
40. Cruz-Martin, A., Crespo, M., and Portera-Cailliau, C. (2010) Delayed stabilization of dendritic spines in fragile X mice. *J. Neurosci.* **30**, 7793–7803
41. van der Zee, E. A. (2015) Synapses, spines and kinases in mammalian learning and memory, and the impact of aging. *Neurosci. Biobehav Rev.* **50**, 77–85
42. Chapleau, C. A., Boggio, E. M., Calfa, G., Percy, A. K., Giustetto, M., and Pozzo-Miller, L. (2012) Hippocampal CA1 pyramidal neurons of Mecp2 mutant mice show a dendritic spine phenotype only in the presymptomatic stage. *Neural Plast.* **2012**, 976164
43. Sowers, L. P., Loo, L., Wu, Y., Campbell, E., Ulrich, J. D., Wu, S., Paemka, L., Wassink, T., Meyer, K., Bing, X., El-Shanti, H., Usachev, Y. M., Ueno, N., Manak, J. R., Shepherd, A. J., *et al.* (2013) Disruption of the non-canonical Wnt gene PRICKLE2 leads to autism-like behaviors with evidence for hippocampal synaptic dysfunction. *Mol. Psychiatry* **18**, 1077–1089
44. Maynard, K. R., and Stein, E. (2012) DSCAM contributes to dendrite arborization and spine formation in the developing cerebral cortex. *J. Neurosci.* **32**, 16637–16650
45. Stachowicz, K. (2018) The role of DSCAM in the regulation of synaptic plasticity: Possible involvement in neuropsychiatric disorders. *Acta Neurobiol. Exp. (Wars)* **78**, 210–219
46. Capecchi, M. R. (2005) Gene targeting in mice: Functional analysis of the mammalian genome for the twenty-first century. *Nat. Rev. Genet.* **6**, 507–512
47. Chen, S., Chen, J., Shi, H., Wei, M., Castaneda-Castellanos, D. R., Bultje, R. S., Pei, X., Kriegstein, A. R., Zhang, M., and Shi, S. H. (2013) Regulation of microtubule stability and organization by mammalian Par3 in specifying neuronal polarity. *Dev. Cell* **24**, 26–40
48. Cao, M., Xu, J., Shen, C., Kam, C., Huganir, R. L., and Xia, J. (2007) PICK1-ICA69 heteromeric BAR domain complex regulates synaptic targeting and surface expression of AMPA receptors. *J. Neurosci.* **27**, 12945–12956
49. Zhao, G. X., Xu, Y. Y., Weng, S. Q., Zhang, S., Chen, Y., Shen, X. Z., Dong, L., and Chen, S. (2019) CAPS1 promotes colorectal cancer metastasis via Snail mediated epithelial mesenchymal transformation. *Oncogene* **38**, 4574–4589
50. Dong, P., Wang, X., Liu, L., Tang, W., Ma, L., Zeng, W., Sun, S., Zhang, L., Zhang, N., Shen, X., Janssen, H., Dong, L., Zhang, S., and Chen, S. (2020) Dampened VEPH1 activates mTORC1 signaling by weakening the TSC1/TSC2 association in hepatocellular carcinoma. *J. Hepatol.* **73**, 1446–1459
51. Liu, X., Yu, X., Zack, D. J., Zhu, H., and Qian, J. (2008) TiGER: A database for tissue-specific gene expression and regulation. *BMC Bioinformatics* **9**, 271
52. Zhang, Y. (2008) I-TASSER server for protein 3D structure prediction. *BMC Bioinformatics* **9**, 40
53. Savojardo, C., Fariselli, P., Martelli, P. L., and Casadio, R. (2017) ISPRED4: Interaction sites PREDiction in protein structures with a refining grammar model. *Bioinformatics* **33**, 1656–1663
54. Yan, Y., Zhang, D., Zhou, P., Li, B., and Huang, S. Y. (2017) HDOCK: A web server for protein-protein and protein-DNA/RNA docking based on a hybrid strategy. *Nucleic Acids Res.* **45**, W365–W373

55. Dai, W., Wu, A., Ma, L., Li, Y. X., Jiang, T., and Li, Y. Y. (2016) A novel index of protein-protein interface propensity improves interface residue recognition. *BMC Syst. Biol.* **10**, 112
56. Kraeuter, A. K., Guest, P. C., and Sarnyai, Z. (2019) The Y-maze for assessment of spatial working and reference memory in mice. *Methods Mol. Biol.* **1916**, 105–111
57. Vorhees, C. V., and Williams, M. T. (2006) Morris water maze: Procedures for assessing spatial and related forms of learning and memory. *Nat. Protoc.* **1**, 848–858
58. Sheng, H., Lv, S., Cai, Y., Shi, W., Lin, W., Liu, T., Lv, N., Cao, H., Zhang, L., and Zhang, Y. (2020) Activation of ventrolateral orbital cortex improves mouse neuropathic pain–induced anxiodepression. *JCI Insight* **5**, e133625
59. Can, A., Dao, D. T., Terrillion, C. E., Piantadosi, S. C., Bhat, S., and Gould, T. D. (2012) The tail suspension test. *J. Vis. Exp.*, e3769
60. Yankelevitch-Yahav, R., Franko, M., Huly, A., and Doron, R. (2015) The forced swim test as a model of depressive-like behavior. *J. Vis. Exp.*, 52587
61. Bian, W. J., Miao, W. Y., He, S. J., Qiu, Z., and Yu, X. (2015) Coordinated spine pruning and maturation mediated by inter-spine competition for cadherin/catenin complexes. *Cell* **162**, 808–822